



## New insights into the stratigraphy and $^{230}\text{Th}/\text{U}$ geochronology of the post-caldera explosive volcanism of La Primavera caldera, Mexico



Delphine Sourisseau<sup>a,\*</sup>, José Luis Macías<sup>b</sup>, Felipe García Tenorio<sup>b</sup>, Denis Ramón Avellán<sup>c</sup>, Ricardo Saucedo Girón<sup>d</sup>, Juan Pablo Bernal<sup>e</sup>, José Luis Arce Saldaña<sup>f</sup>, Zareth Tinoco Murillo<sup>g</sup>

<sup>a</sup> Posgrado en Ciencias de La Tierra, Escuela Nacional de Estudios Superiores Unidad Morelia, Universidad Nacional Autónoma de México, Antigua Carretera a Pátzcuaro 8701, 58190, Morelia, Michoacán, Mexico

<sup>b</sup> Instituto de Geofísica, Universidad Nacional Autónoma de México, Antigua Carretera a Pátzcuaro 8701, 58190, Morelia, Michoacán, Mexico

<sup>c</sup> CONACYT – Instituto de Geofísica, Universidad Nacional Autónoma de México, Antigua Carretera a Pátzcuaro 8701, 58190, Morelia, Michoacán, Mexico

<sup>d</sup> Universidad Autónoma de San Luis Potosí, Instituto de Geología/Fac. Ingeniería, Av. Manuel Nava No 5, Zona Universitaria, 78240, San Luis Potosí, S.L.P., Mexico

<sup>e</sup> Centro de Geociencias, Universidad Nacional Autónoma de México, Unidad Juriquilla, Juriquilla, Mexico

<sup>f</sup> Instituto de Geología, Universidad Nacional Autónoma de México, Ciudad de México, Mexico

<sup>g</sup> Maestría en Geociencias y Planificación Del Territorio, Instituto de Investigaciones en Ciencias de La Tierra, Universidad Michoacana de San Nicolás de Hidalgo, 58066, Morelia, Michoacán, Mexico

### ARTICLE INFO

#### Keywords:

La primavera caldera  
Post-caldera volcanism  
Stratigraphy  
 $^{230}\text{Th}/\text{U}$  dating  
Caldera evolution

### ABSTRACT

La Primavera caldera is a Quaternary rhyolitic volcanic field located in the western part of the Trans-Mexican-Volcanic-Belt (TMVB). The caldera forming eruption of La Primavera occurred ~95 ka with the emplacement of the Tala ignimbrite. Here, we present a new stratigraphy and evolution of the post-caldera activity based on intense fieldwork, correlation of deposits, and ten  $^{230}\text{Th}/\text{U}$  geochronology dates in zircons. The collapse produced an 11-km wide caldera followed by the formation of an intra-caldera lake. After the caldera collapse, several rhyolitic domes were extruded, inside and outside the caldera ring-fault until 26.8 ka. The first post-caldera pyroclastic event took place 86.4 ka with the eruption that emplaced the Giant Pumice (GP) followed by the occurrence of at least fourteen pyroclastic units (UA to UN). The intra-caldera explosive activity came from the central resurgent Nejahuite composite dome with the deposition of the GP and A to D units between 86.4 and 71.5 ka. The extra-caldera explosive activity came from the San Miguel, Planillas and Tajo volcanic centers with the deposition of the E to N units inside the caldera and south of the caldera ring fault between 71.5 and 26.8 ka. Three eruptions were originated at San Miguel volcanic center between 71.5 and 60.3 ka (units E, G and H) and six eruptions dated between 68.9 and 44.7 ka were originated at Planillas volcanic center (units F, I, J, K, L and M). The last eruption of the caldera occurred between 44.7 and 26.8 ka at the Tajo volcanic center (UN). The eruptions appear as pyroclastic successions interbedded with lake deposits (units GP and A-B) and as subaerial deposits separated by paleosols or lahar deposits (units C-M). The revised stratigraphy indicates that the caldera resurgence occurred right after the caldera collapse 93.8 ka and continued until 75.8 ka. This new pyroclastic stratigraphy provides key information on the post-caldera evolution of La Primavera.

### 1. Introduction

The process of dome resurgence is a common feature of post-caldera evolution. This phenomenon is caused by the uplift of the caldera floor by extensive magmatic intrusions through fractures and faults formed during the caldera collapse or older reactivated faults related to regional tectonism (Smith and Bailey, 1968; Kennedy et al., 2012). This process leads to the extrusion of lava domes inside the caldera with the uplift of

older successions of rocks for instance Valles caldera (Smith and Bailey, 1968; Phillips et al., 2007), Nisyros (Di Paola, 1974), and Lake City caldera (Hon and Lipman, 1989). In some cases, magma resurgence take place outside the caldera ring-fault as it was documented in calderas as Nisyros Island (Di Paola, 1974), Taupo in New Zealand (Cole and Spinks, 2009) and Long Valley in California (Bailey et al., 1976). Sometimes, resurgence can lead to explosive activity after the caldera collapse as documented at Valles caldera in New-Mexico (Wolff and Gardner,

\* Corresponding author.

E-mail address: [d.sourisseau@igeofisica.unam.mx](mailto:d.sourisseau@igeofisica.unam.mx) (D. Sourisseau).

1995), Aso caldera in Japan (Miyabuchi, 2009, 2011), Cinque Denti caldera in Italy (Jordan et al., 2018), and the Acoculco caldera in Mexico (Avellán et al., 2019). This activity can disperse thick-widespread deposits that cover previous successions and the caldera ring-fault making it difficult to understand the caldera stratigraphy and evolution.

This is the case of the  $\approx$ 95 ka La Primavera Caldera formed by a large explosive eruption that emplaced the rhyolitic Tala ignimbrite (Mahood, 1977; Mahood, 1980, 1981). These authors presented the first geological map of La Primavera and recognized a large number of lava flows and domes. This geologic map was then supported by a particularly good set

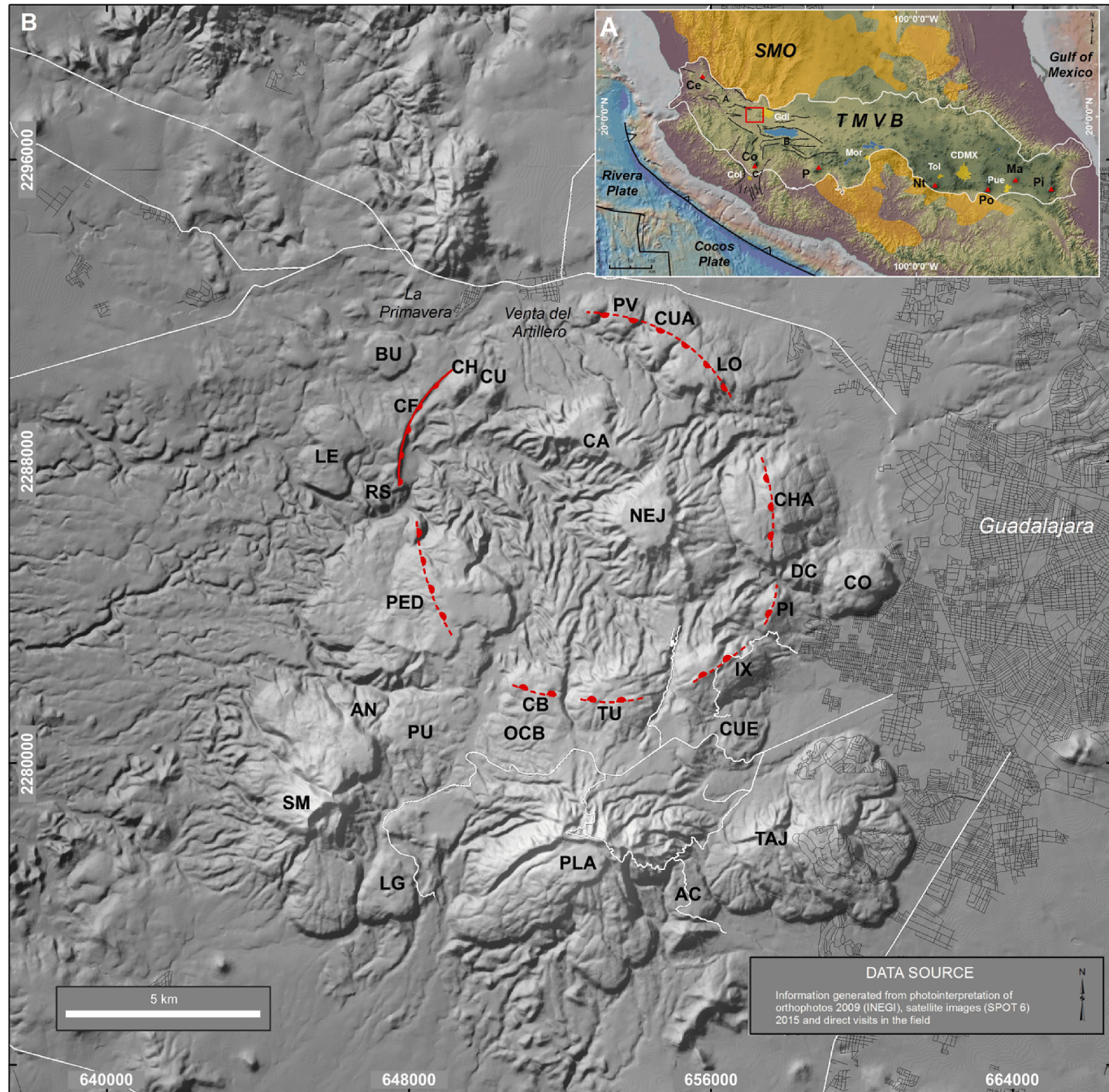


**Fig. 1.** A) Sketch map that shows the present tectonic plate configuration and the extent of the Sierra Madre Occidental (SMO) and the Trans-Mexican Volcanic Belt (TMVB). La Primavera caldera (red square) is located on the western part of the TMVB. The World Geodetic System WGS 84 ellipsoid is used in the UTM 13 coordinate system at 1 : 100,000 scale. A: Tepic-Zacoalco Graben; B: Chapala Graben; C: Colima Graben. Volcanic centers are: Ce = Ceboruco; Co = Colima; P = Parícutin; Nt = Nevado de Toluca; Po = Popocatépetl; Ma = Malinche; and Pi = Pico de Orizaba. Cities: Gdl = Guadalajara; Col = Colima; Mor = Morelia; Tol = Toluca; CDMX = Ciudad de Mexico; Pue = Puebla. B) Shaded relief model of LP with the location of lavas, domes, and volcanic centers. The continuous and dotted red lines indicate the trace of the visible and inferred caldera ring-fault, respectively. Grey lines represent the streets of main cities and towns, and white lines the main roads in the area. Abbreviations are: Lava: CF = Cañón de las Flores and LG = Llano Grande. Domes: AC = Arroyo Colorado, AN = Animas, BU = Burro, CA = Cerro Alto, CHA = Chapulin, CH = Chato, CO = Colli, CU = Cuate, CUA = Cuartilla, CUE = Cuesta, CB = Culebreado, DC = Dos Coyotes, IX = Ixtahuatonte, LE = Léon, LO = Lobera, OCB = Old Culebreado, PED = Pedernal, PI = Pilas, PV = Piñar de la Venta, PU = Puerta, RS = Rio Salado and TU = Tule. Volcanic center: NEJ = Nejahuete, PLA = Planillas, SM = San Miguel and TAJ = Tajo. (Color online, 2 column fitting image). (For interpretation of the references to colour in this figure legend, the reader is referred to the Web version of this article.)

of 46 K–Ar dates that allowed them to propose a general evolution scheme of the caldera (Mahood and Drake, 1982). However, these authors did not provide a stratigraphic correlation of the effusive eruptions (lava flows and final domes) with the multiple successions of pyroclastic deposits.

The first attempt to understand the pyroclastic stratigraphy of LP was presented by Walker et al. (1981). These authors correlated the deposits of twelve stratigraphic sections inside and outside the caldera. They recognized ten main fall deposits named from A to J, B being the co-ignimbrite ash fall of the Tala ignimbrite. They used the B, E and J deposits as a reference to correlate the stratigraphic sections. With the construction of isopach and isopleths maps of the D, F and J deposits, the authors proposed that all young fallouts have been sourced at the San Miguel and Planillas satellite volcanoes. Unfortunately, the authors gave extremely poor description of the deposits (i.e. structure and components) and no age constraints making difficult to correlate their results to our new results. In this study, we carried out intense fieldwork and componentry analyzes to establish the post-caldera stratigraphy of La Primavera. New  $^{230}\text{Th}/\text{U}$  dates in zircons were used to provide meaningful ages of the pyroclastic deposits and support the reconstruction of the post-caldera stratigraphy. With all this information, we present a detailed stratigraphy of the post-caldera evolution of La Primavera that occurred between  $\approx$ 95 and 26.8 ka, and a better timing of the caldera resurgence.

## 2. Geologic background

The LP is a late Pleistocene 11-km wide caldera that sits near the intersection between two large volcanic provinces in Mexico, the Sierra Madre Occidental (SMO) and the Trans-Mexican-Volcanic-Belt (TMVB) (Rossotti et al., 2002) (Fig. 1). The SMO is a 20–31.5 Ma silicic volcanic province emplaced during the subduction of the Farallon plate beneath the North American plate (Ferrari et al., 2002). The TMVB is a continental volcanic arc associated to the subduction of the Rivera and Cocos plates beneath the North American plate at the Middle American Trench (Nixon, 1982; Luhr et al., 1985; DeMets and Stein, 1990). Locally, the caldera is situated at  $\approx$ 50 km north of the triple point junction formed by the N–S Colima, the E–W Chapala, and the NW–SE Tepic Zacoalco grabens (Luhr et al., 1985) (Fig. 1).

LP is located within the Tepic-Zacoalco graben among other Quaternary volcanic structures as Tequila and Ceboruco volcanoes to the northwest (Ferrari et al., 2000a, 2000b), the lavas and cinder cones of the Southern Guadalajara Volcanic Chain (Luhr and Lazaar, 1985), and the ignimbrites of the SMO to the east (Ferrari et al., 2002). According to the drill hole stratigraphy (i.e. PR9 well) conducted by the National Power Company (Comisión Federal de Electricidad = CFE) (Santoyo-Gutiérrez et al., 1991; Rosas-Elguera et al., 1997), the LP sits on top of a sequence made of Cretaceous granite located at a depth of  $\sim$ 3 km, andesitic lavas ( $51 \pm 2.5$  Ma), a rhyolitic ignimbrite, basalts and basaltic-andesite lavas of the San Cristobal group ( $12.5 \pm 0.6$  Ma), the rhyolite and ash flow deposits of the Guadalajara group (7.15–3.1 Ma; Gilbert et al., 1985; Moore et al., 1994), an andesitic lava, and an ash-flow tuff ( $1.6 \pm 0.2$  Ma).

The evolution of the LP was extensively described in several studies of Mahood and coworkers (Mahood, 1977; Mahood, 1980, 1981; Mahood, 1981a, 1981b; Mahood and Drake, 1982). These authors described the evolution of the caldera based on their geologic mapping, stratigraphy, chemistry, and K/Ar dating of rocks. They divided its evolution in pre-caldera, syn-caldera (Tala Tuff), and post-caldera (Central domes, Giant Pumice Horizon (GPH), Older ring domes, Younger ring domes and Southern arc lavas) and categorized the volcanoes as dome, composite dome, and volcanic center. Based on this stratigraphy Mahood and coworkers (Mahood, 1981a; Mahood and Drake, 1982) proposed an evolution model of the caldera. In their model they considered that pre-caldera lavas were emplaced from 145 to 100 ka. At around 96.7–95.2 ka, the collapse of the roof magma reservoir

produced an 11-km wide caldera depression (La Primavera caldera) during which  $20 \text{ km}^3$  of magma dispersed the Tala ignimbrite, the Central resurgent domes, the Giant Pumice Horizon and Older ring domes were emplaced  $\approx$  95 ka, followed by the extrusion of the Younger ring domes  $\approx$  75 ka and the Southern arc lavas between 60 ka and 25 ka.

All rocks of LP have a high-silica rhyolite composition (>75 wt% SiO<sub>2</sub>) with some variations in the mineralogy (Mahood, 1977; Mahood, 1981a; Mahood, 1981b). These authors concluded that the Tala ignimbrite was zoned from base to top from mildly peralkaline to metaluminous compositions. Nejahuete and the earliest post-caldera domes have more or less the same composition than the upper part of the Tala ignimbrite. In contrast, the Cerro Alto dome has a more transitional signature. The 75, 60 and 30 ka post-caldera domes become progressively less peralkaline. Domes, the GPH, and the Tala ignimbrite are aphyric with less than 15% of sanidine > quartz > Fe-hedenbergite > fayalite > ilmenite + titanomagnetite phenocrysts. However, some domes also have titanomagnetite, apatite, and chevkinite crystals (Vazquez et al., 2014).

## 3. Material and analytical methods

### 3.1. Digital resources

We used the digital topography of the National Institute of Statistics, Geography, and Informatics (INEGI, 2009–2010), nine topographic maps scale 1: 50,000 (F13D54, F13D55, F13D56, F13D64, F13D65, F13D66, F13D74, F13D75 and F13D76), 54 panchromatic orthophotos scale 1: 20,000 (1.5 m of resolution; i.e. F13D54A, B, C, D, E and F), a satellite image from SPOT 7 with resolution panchromatic 1.5 m and multispectral image of 6 m of resolution (2015) with the World Geodetic System (WGS 84 ellipsoid) in the UTM 13 coordinate system. Then altitude, slope and shaded maps were produced from the corrected topographic map using the interpolation method with cloud points of the ArcMap 10.2 software. Finally, the altitude map (20 m level curves) obtained was used to build DEM and shaded DEM with 15 m of resolution to characterize the relief shapes and elements present on the map (Fig. 2).

### 3.2. Sampling

Circa of 600 sites were studied in the field between August 2015 and November 2018 (Fig. 2). At each location we described the deposit structure (thickness, geometry, limits), texture (clast size, grading), and componentry (clast type, mineralogy) of the pyroclastic deposits. Fallout and some dense PDC deposits were sampled for grain size, componentry, geochemistry, and radiometric analysis. The geochemical data will be presented and interpreted in another publication. Eighty-four samples were sieved from -5Φ to 4Φ, in 1Φ spaced intervals, to get the granulometric median diameter (Md<sub>φ</sub>) and the graphical standard deviation ( $\sigma_\Phi$ ) of Inman (1952). We selected thirty samples to display grain size distributions and componentry of the pyroclastic units. Whenever more than one sample was collected from each unit (X) we aggregate a suffix (a-c) to name the samples (see Supplementary material table 1). For the componentry analysis, we counted between 500 and 1000 fragments of samples of the 1<sub>φ</sub> sieve fraction. The components were described as juvenile pumice, blocky juvenile fragment, lithic and crystal.

### 3.3. Zircon extraction and $^{230}\text{Th}/\text{U}$ analysis

All pumices were cleaned using water and cutter to remove small fragments, ashes, soil and lichen present on the crust and inside vesicles. Then they were washed using ultrasonic cleaner and distilled water until getting clear water. Depending on their conditions of freshness, all samples were cleaned at least 3 times for 5 min and dried in an oven 24 h at 60 °C. Then all samples were placed in separate plastic bags and crushed with a hammer until the fraction 3<sub>φ</sub> (0.125 mm sieve mesh) and

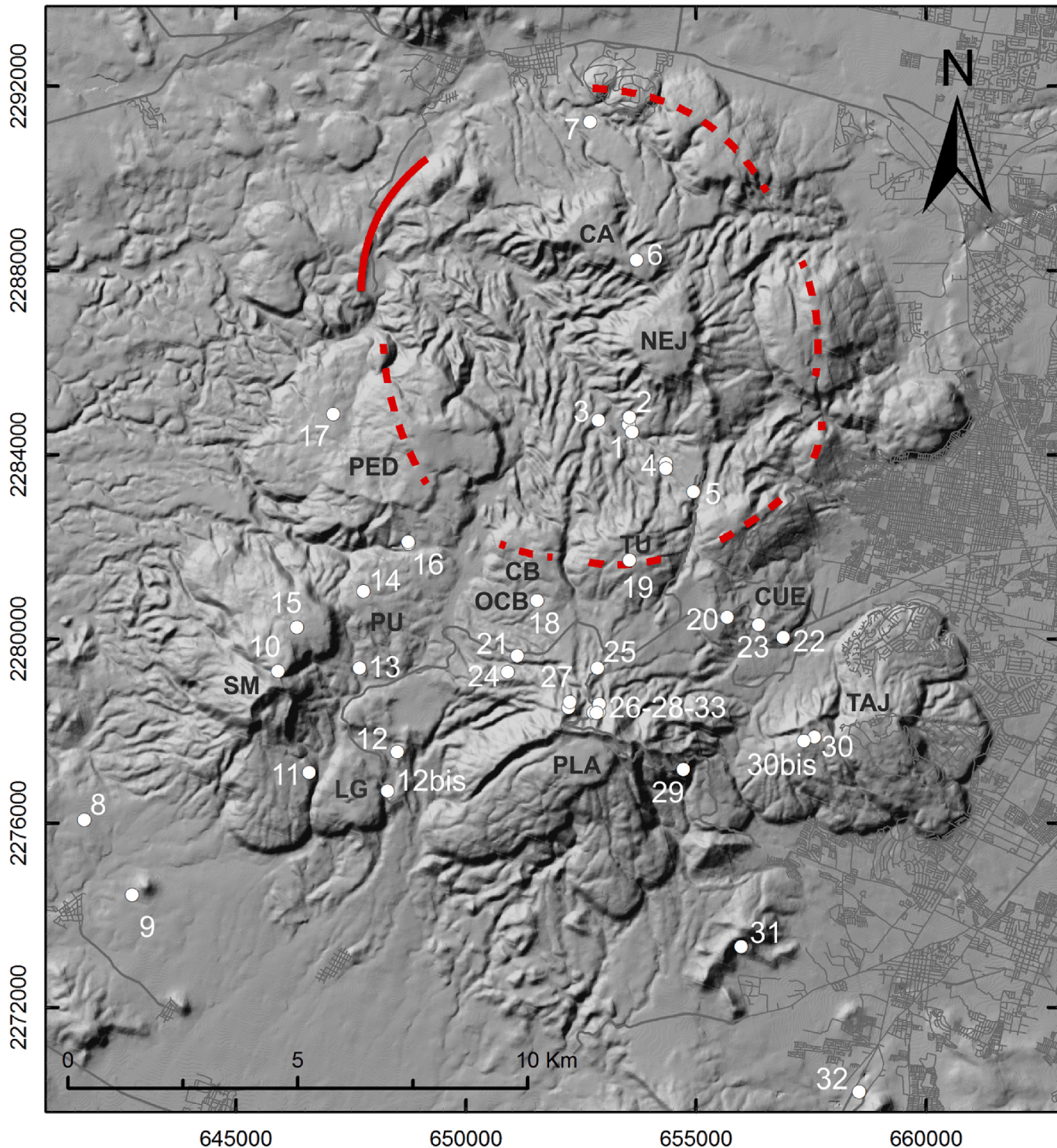


**Fig. 2.** DEM of LP showing the main volcanic structures (after Mähood, 1981a). Stratigraphic sections are represented by white circles with numbers. The red and dotted red lines indicate the visible and inferred caldera ring-fault, respectively. The grey lines represent the streets of main cities and towns. Abbreviations are the same as in Fig. 1. (Color online, 2 column fitting image). (For interpretation of the references to colour in this figure legend, the reader is referred to the Web version of this article.)

sieved at the fraction 2.5φ (0.177 mm sieve mesh). From the powder obtained, zircons were separated under the binocular microscope.

The zircon grains from each sample were mounted on epoxy resin, polished, and analyzed by LA-MC-ICPMS for  $(^{238}\text{U}/^{232}\text{Th})$ ,  $(^{230}\text{Th}/^{232}\text{Th})$  following Bernal et al. (2014), using a Thermo Finnigan Neptune-Plus MCICPMS attached to a Resonetics L-50 laser-ablation workstation (Müller et al., 2009; Solari et al., 2010), projecting a 44

μm diameter laser at the surface, with a ~6 J/cm<sup>2</sup> fluence. The results were reduced using the software Iolite 3.0 (Paton et al., 2011) and the isochron ages, uncertainties and MSWD were calculated using Isoplot R (Vermeesch, 2018). The ages were obtained, when applicable, from  $(^{230}\text{Th}/^{232}\text{Th})$  vs.  $(^{238}\text{U}/^{232}\text{Th})$  isochrons using the decay constants from Jaffey et al. (1971) for  $^{238}\text{U}$ , and Cheng et al. (2013) for  $^{230}\text{Th}$ . The U-Th raw data are given in the Supplementary material table 2.

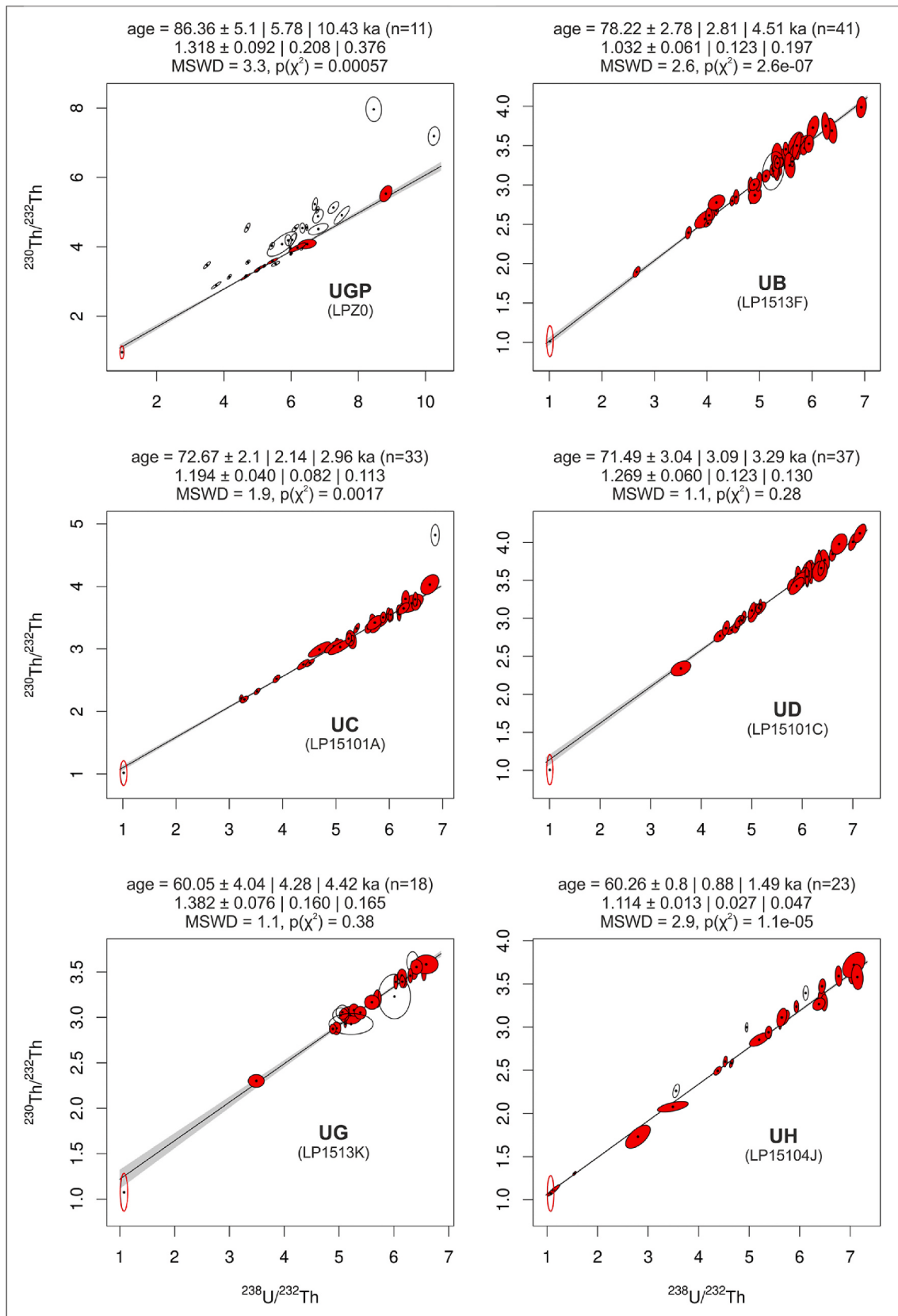


**Fig. 3.**  $^{230}\text{Th}/\text{U}$  isochrons plots of in-situ zircon dates of post-caldera units from GP to M. The isochron ages are shown with the 2 $\sigma$  analytical uncertainties. Red filled ellipses: zircons used in the isochron age calculations. Red empty ellipses: sample whole rock compositions. White ellipses: zircons not used in the isochron age calculations. Grey lines: inferred isochrons. Data-point error ellipses are 2 $\sigma$ . (Color online, 2 column fitting image). (For interpretation of the references to colour in this figure legend, the reader is referred to the Web version of this article.)

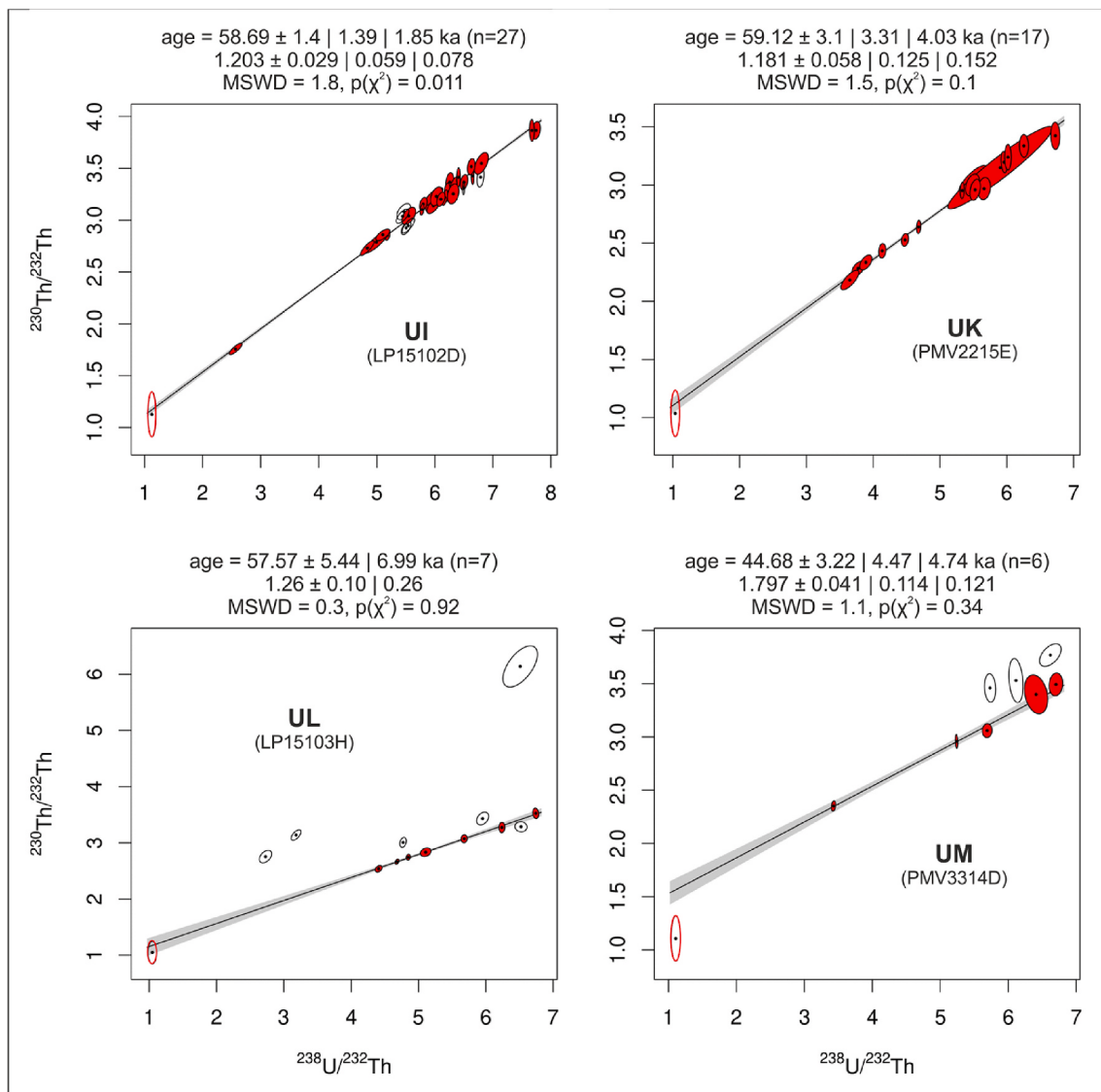


Fig. 3. (continued).

Pumice fragments from each sample were selected, washed in distilled water, dried and crushed using a hammer and pulverized in tungsten carbide plates. U and Th elements were determined by Fusion Mass Spectrometry (FUS-MS) at Activation Laboratories, Ancaster, Canada. The limit of detection (LOD) is less than 0.05 ppm for Th and less than 0.01 ppm for U. The analytical precision is generally better than 10%. From those results, the ( $^{230}\text{Th}/^{232}\text{Th}$ ) and ( $^{238}\text{U}/^{232}\text{Th}$ ) activity ratios were calculated from the  $^{232}\text{Th}$  and  $^{238}\text{U}$  decay constants and natural abundances (Supplementary material table 3).

#### 4. Zircon $^{230}\text{Th}/\text{U}$ ages

Ten  $^{230}\text{Th}/\text{U}$  isochron ages were obtained to constrain the age of the LP post-caldera deposits (Fig. 3). The isochron ages, number of zircons analyzed, and MSWD from units GP-M used in the stratigraphic correlations are listed in Table 1.

#### 5. Terminology

We described four types of pyroclastic deposits in the stratigraphic succession of LP that we interpret as follows:

*Pyroclastic fall:* well sorted and clast-supported layers with flat or

Table 1

$^{230}\text{Th}/\text{U}$  isochron age of units GP-M. The results are shown with  $2\sigma$  analytical uncertainties. (white and black, 2 column fitting table).

Unit	Sample	Section	$^{230}\text{Th}/\text{U}$ Isochron ages (ka)			
			Age	+/-	MSWD	N
GP	LPZ0	1 bis	86,4	5,1	3,3	11
B	LP1513F	3	78,2	2,8	2,6	41
C	LP15101A	20	72,7	2,1	1,9	33
D	LP15101C	20	71,5	3,0	1,1	37
G	LP1513K	3	60,1	4,0	1,1	18
H	LP15104J	8	60,3	0,8	2,9	23
I	LP15102D	22	58,7	1,4	1,8	27
K	PMV2215E	31	59,1	3,1	1,5	17
L	LP15103H	23	57,6	5,4	0,3	7
M	PMV3314D	32	44,7	3,2	1,1	6

planar contacts of lapilli-to-coarse-ash components deposited by fallouts from eruptive columns.

*Wet surges:* thin cross-bedded layers formed by fine to medium-grained ash with basal erosive contacts emplaced from dilute Pyroclastic Density Currents (PDC). They are more compacted and with limited distribution in the field. Some of these layers present dune

structures and impact deformations.

**Dry surges:** friable, stratified to cross-bedded layers of fine lapilli to fine ash with basal erosive contacts emplaced from dilute PDC.

**Pyroclastic flow:** massive, poorly to very poorly sorted, matrix-supported layers made of block to lapilli-size pumice and lithics set in a fine ash matrix dispersed by dense PDC.

## 6. Post-caldera stratigraphy

Based on the correlation of 30 selected stratigraphic sections (Fig. 2) and supported by componentry analysis and new  $^{230}\text{Th}/\text{U}$  dates (Fig. 3), we identified 14 pyroclastic units younger than the Giant Pumice (86.4 ka). The compound stratigraphic column of Fig. 4 shows these units named from UA to UN. Units GP to C are separated by lacustrine deposits dubbed as units ML1, ML2 and UL. Next, we described each unit from older to younger.

### 6.1. Giant pumice unit (UGP)

This unit was first called Giant Pumice Horizon by Mahood and co-workers (Mahood, 1977; Clough et al., 1981). It is exposed inside the caldera between the Lower Lacustrine Unit (ULL) and the Middle Lacustrine 1 Unit (UML1) (Fig. 5A and 10). It is a whitish to grey continuous thick bed (4–12 m) that makes an excellent stratigraphic marker. UGP is made of white to grey pumice clasts embedded in fine-grained ash matrix and lacustrine sediments with diatoms. Individual pumice blocks made of up to 80 vol% of the layer varying in diameter between 0.3 and 6 m (Tinoco Murillo, 2017). A sample of a single pumice from the base of UGP yielded a zircon  $^{230}\text{Th}/\text{U}$  isochron age of  $86.4 \pm 5.1$  ka at section 1bis south of the Nejahuete composite dome (Table 1).

### 6.2. Unit A (UA)

UA occurs in three sections located inside the caldera. It occurs between UML1 and the Middle Lacustrine 2 Unit (UML2) with plane sharp contacts and variable thicknesses (6.2–8.2 m) (Figs. 5B and 10). We will only present the general characteristics of the deposit given the impossibility to access and describe at close range most outcrops. The best exposure of UA occurs at section 3 south of the Nejahuete composite dome. Here, it can be divided in two parts: UA1 (3.4 m) is a grey, parallel stratified lacustrine deposit made of clay and ash particles, and UA2 (5 m) is a succession of grey cross-stratified coarse ash surge layers, pyroclastic fall deposits made of medium to coarse ash pumice (A2 Xb section 4bis), and pyroclastic flow deposits made of fine to medium lapilli pumice and lithics set in a coarse ash matrix (A2 Xa section 4bis, and A2 Xc section 3) with occasional white thin clayed lacustrine beds with parallel stratification. The contact between UA1 and UA2 is plane sharp to locally erosive with oxidation and desiccating cracks. This unit lies between GPU ( $86.4 \pm 5.1$  ka) and a lava of the Upper Nejahuete dome dated at 82.8 ka (Mahood, 1980; Mahood and Drake, 1982).

### 6.3. Unit B (UB)

UB is exposed in four stratigraphic sections inside the caldera, and on top of the Old Culebreado (OCB) and Tule domes close to the southern caldera ring fault. It is grey on top of the Cerro Alto dome, OCB and Tule domes and orange to grey in exposures inside the caldera. It usually lies between units UML2 and a lahar deposit with an erosive contact below the Upper Lacustrine Unit (UUL) and a maximum thickness of 10.5 m in section 3 (Fig. 5C and 10). In this section, located south of Nejahuete, UB can be subdivided in two parts: The basal part UB1 (4 m) consists of white parallel stratified, clayed lacustrine beds alternating with grey laminated surge layers made of medium to coarse ash, some layers are oxidized. UB2 (6.3 m) consists of a succession of oxidized, diffuse stratified thin pyroclastic fall deposits with coarse ash to medium lapilli

pumice (B2 Xa, Xb, and Xc section 6) alternating with massive pyroclastic flow deposits and thick surge layers that contain coarse lapilli to fine block pumice and lithics set in a medium to fine ash matrix. The contact between UB1 and UB2 is plane sharp to locally erosive with an oxidation layer. Pumice fragments ( $-1$  to  $-3$  φ) of the basal subunit UB2 yielded a zircon  $^{230}\text{Th}/\text{U}$  isochron age of  $78.2 \pm 2.8$  ka at section 3 south of the Nejahuete composite dome (Table 1).

### 6.4. Unit C (UC)

This unit overlies UUL and a lahar deposit with a sharp erosive contact and underlies a lahar deposit and unit D (Figs. 5D and 10). The only in situ outcrops of UC occur on the road between the Tule and Cuesta domes (section 5) and atop the Cuesta dome (section 20). It usually occurs as reworked deposits (lahar) in most locations inside the caldera. In section 5, UC can be divided from base to top in two grey sub-units: UC1 (7.9 m) is a succession of five pyroclastic flow deposits made of fine to medium pumice and lithics supported by a coarse ash matrix (C1 Xa and Xb), and UC2 (1 m) is a diffuse stratified well-sorted (C2 Xc) pyroclastic fall deposit with coarse ash to fine lapilli pumice. The contact between UC1 and UC2 is plane sharp. Part of UC was also found on the Tule and Cuesta domes on the southern part of the caldera (sections 19 and 20). Pumice fragments ( $-1$  to  $-2$  φ) from subunit UC2 collected at section 20 on the Cuesta dome gave a  $^{230}\text{Th}/\text{U}$  isochron age in zircons of  $72.7 \pm 2.1$  ka (Table 1).

### 6.5. Unit D (UD)

This unit was described in eight stratigraphic sections atop the Nejahuete composite dome and atop the Culebreado, Old Culebreado, Tule, and Cuesta domes on the southern part of the caldera. UD usually lies between units C and E (Fig. 5E and 10) and covers lahars deposits developed from unit C with an undulated sharp contact at section 20. The best outcrop of UD was found at section 20 on the Cuesta dome that consists of a 2.1 m thick white diffuse stratified pyroclastic fall deposit made of fine to medium lapilli pumice. A sample of pumice fragments collected at the base of this unit at section 20 on top of the Cuesta dome yielded a  $^{230}\text{Th}/\text{U}$  isochron age in zircons of  $71.5 \pm 3.0$  ka that correlates with its stratigraphic position (Table 1).

### 6.6. Unit E (UE)

This unit was first described by Cruz Lara (2015). UE occurs in 11 stratigraphic sections exposed on the San Miguel volcanic center, old Culebreado, Culebreado and Tule domes, and at the northern basal flank of the Planillas volcanic center. It lies between units D and F on the Old Culebreado dome (section 18) and below unit G south of the San Miguel volcanic center (section 8) (Fig. 7A,C-D, and 10). The thickest outcrop of this unit (6.7 m) was found at section 10 on top of San Miguel volcano. UE lies atop a 5.7 cm paleosol developed from the UD deposits on the Old Culebreado dome (section 18). At section 12, UE can be divided from base to top in two sub-units: UE1 (2.6 m) is made of thin cross-stratified wet surge layers alternating with lenses of pyroclastic flow deposits and multiple reverse graded pyroclastic fall made of fine to medium pumice. UE2 (4 m) consists of a set of four multiple reverse graded pyroclastic fall deposits (E2 Xa, Xb and Xc) made of coarse ash to medium lapilli pumice separated by thin cross-stratified wet surge layers with medium to coarse ash fragments. The contact between UE1 and UE2 is plane sharp to locally erosive. We did not obtain an age for this unit but it lies between unit D ( $71.5 \pm 3.0$  ka) and the Upper Pedernal lava dated at 68.9 ka (Mahood, 1980; Mahood and Drake, 1982).

### 6.7. Unit F (UF)

This unit was first called unit C by Walker et al. (1981), it lies between units E and G with a variable thickness (0.35–6.5 m) (Fig. 6A–C,E,

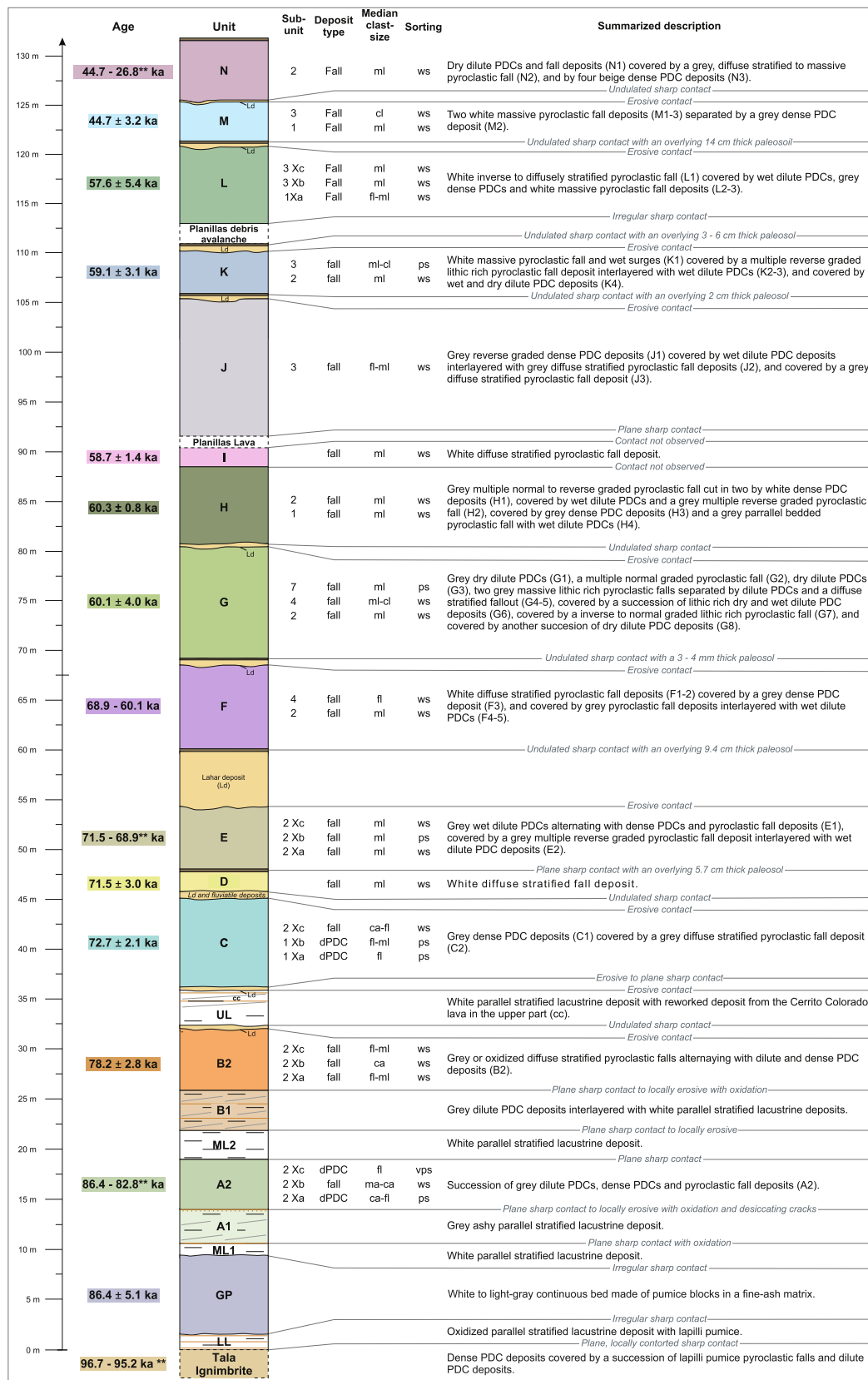


**Fig. 4.** Compound stratigraphic column of the post-caldera pyroclastic deposits, lahar deposits, paleosols and isochron ages. Summarized descriptions of deposits, clast-size and sorting of some deposits are also shown. Abbreviations are coarse ash (ca), fine-grained lapilli (fl), medium-grained lapilli (ml), coarse-grained lapilli (cl), very poorly sorted (vps), poorly sorted (ps), and well sorted (ws) (from Sohn and Chough, 1989). Dates of the Tala Ignimbrite and some units (\*\*) taken from Mahood and Drake (1982). Thicknesses of all units are to scale except for the Tala Ignimbrite (TIU). (Color online, 2 column fitting image). (For interpretation of the references to colour in this figure legend, the reader is referred to the Web version of this article.)

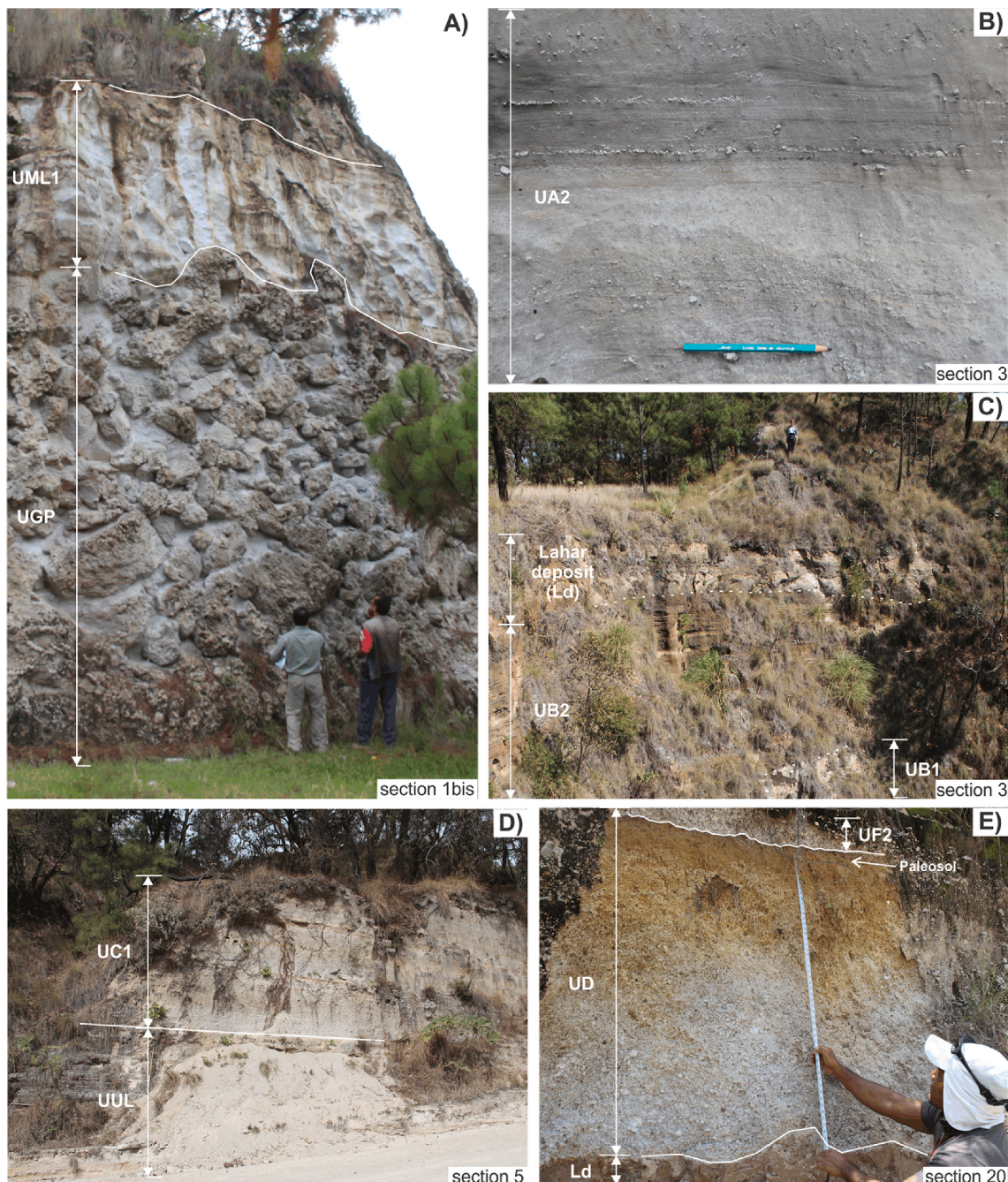


**Fig. 5.** Pictures illustrating main aspects of La Primavera pyroclastic GP-D units. A) Proximal view of the GP with large pumice blocks covered by the UML1 lacustrine deposits. B) Proximal pyroclastic flow and dry surge deposits of UA2. C) Proximal outcrop showing the lacustrine and grey surge deposits from the B1 subunit, and pyroclastic fall and surge deposits from B2. D) Distal outcrop showing the UUL lacustrine deposits and UC1 pyroclastic flow deposits. E) Distal outcrop showing the UD pyroclastic fall and a marron paleosol bellow UF2. The white continuous and dashed lines mark the approximated boundaries between units. (Color online, 2 column fitting image). (For interpretation of the references to colour in this figure legend, the reader is referred to the Web version of this article.)

and 10). UF was described at thirteen sections most of which exposed on the basal part of the Planillas volcanic center, atop the Puerta, Pedernal, Old Culebreado, Culebreado, Tule, and Cuesta domes, and inside the caldera. UF covers lahars deposits (~6 m thick) with an undulated sharp contact inside the caldera and lies atop a 9.4 cm paleosol developed from a lahar deposit on the lower lavas of Planillas volcano (section 21). Here, UF can be divided in four sub-units: UF1 (1 m) consists of a white diffuse stratified pyroclastic fall with coarse ash to fine lapilli pumice. UF2 (5 m) is a white diffuse stratified pyroclastic fall deposit with fine to coarse lapilli pumice and a lithic-rich base. UF3 (1.5 m) is a grey massive pyroclastic flow deposit with a medium to coarse ash matrix. Most of UF4

was eroded on the Planillas volcanic center, however, on the Cuesta dome at section 20, UF4 (1.3 m) consists of grey diffuse stratified pyroclastic falls with coarse ash to fine lapilli pumice alternating with occasional thin fine ash wet surges. UF5 (0.6 m) consists of thin fine ash wet surge layers alternating with pyroclastic fall deposits with fine lapilli pumice. The contacts between subunits are usually plane sharp and plane sharp to locally erosive. We did not obtain an absolute age for this unit, however, its stratigraphic position indicates that it lies between the Upper Pedernal lava dated at 68.9 ka (Mahood, 1980; Mahood and Drake, 1982) and unit G ( $60.1 \pm 4.0$  ka).



**Fig. 6.** Pictures illustrating main aspects of the F-G pyroclastic units. A) Distal diffuse stratified pyroclastic fall and wet surge deposits from the F4 and F5 subunits. B–C) Proximal outcrop illustrating the F1-2 diffused stratified pyroclastic fall and F3 pyroclastic flow deposits. Undulated sharp contact between the UF1 pyroclastic fall and the underlying paleosol and lahar deposit. D–F) Proximal pyroclastic fall, flow, and surge deposits from the G2–8 subunits. Upper part of UG8 eroded by the white pyroclastic flow deposit from UH1bis. Discordance between the F2 and G4 pyroclastic fall deposits. The white lines mark the approximated boundaries between units. (Color online, 2 column fitting image). (For interpretation of the references to colour in this figure legend, the reader is referred to the Web version of this article.)

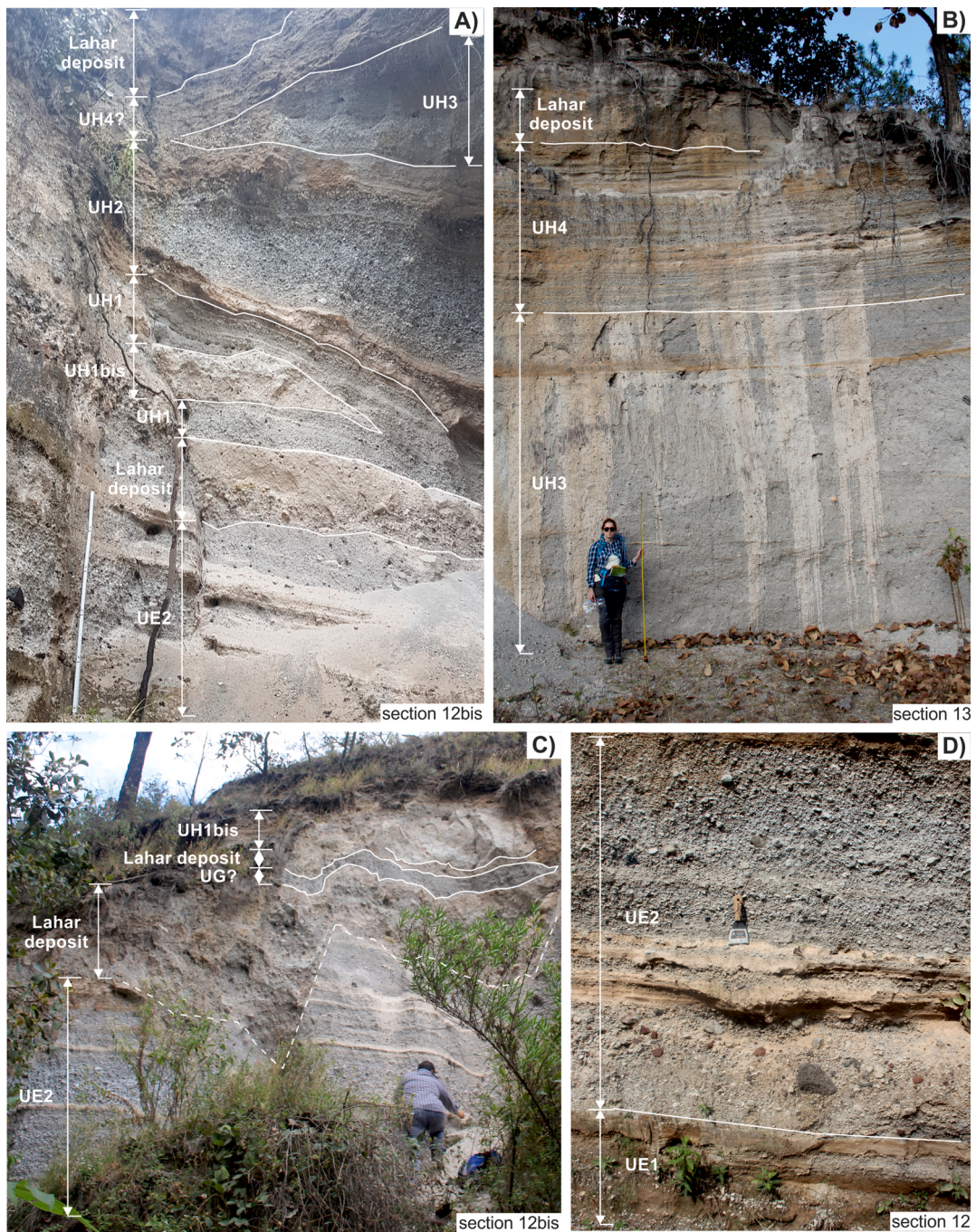


**Fig. 7.** Pictures illustrating proximal outcrops of the E and H pyroclastic units. A) Pyroclastic fall, wet surges and pyroclastic flows from subunits E2, and H1-4. Lahar deposits stands between subunits E2-H1 and on top of H4 with sharp erosive contacts. B) H3 grey pyroclastic flows, and H4 parallel bedded pyroclastic fall and wet surge deposits. The upper part of H4 is reworked by a lahar deposit. C) Sharp erosive contact between a lithic-rich lahar deposit and the UE2 pyroclastic fall and wet surges. Irregular sharp contact between the lahar and the grey pyroclastic deposits possibly from UG. The UG and the UH1bis white pyroclastic flow deposits are separated with an erosive contact by a thin lahar deposit. D) Wet surges and pyroclastic fall deposits from subunits E1-2. The white lines mark the approximated boundaries between units. (Color online, 2 column fitting image). (For interpretation of the references to colour in this figure legend, the reader is referred to the Web version of this article.)

#### 6.8. Unit G (UG)

This unit was first called unit D by Walker et al. (1981), it lies between units F and I on the Cuesta dome at section 22, and bellow unit H on the Puerta dome at section 14 and 16 (Fig. 6D-F, 7C, and 10). UG is exposed atop the Puerta, Pedernal, Old Culebreado, Culebreado, Tule and Cuesta domes on the southern part of the caldera and on top of Cerro Alto dome and Nejahuete composite dome with variable thickness (0.45–6.7 m). UG covers with an undulated sharp contact and paleosol

(3–4 cm thick) derived from a lahar deposit atop UF on the Cuesta dome (section 20). The best exposure of UG observed on the Puerta dome (sections 16 and 16 bis) can be divided in eight sub-units from base to top as: UG1 ( $\leq 6$  m) is formed of coarse ash dry surge layers, UG2 (1.6 m) is a grey pyroclastic fall with multiple normal gradeing made of fine to medium lapilli pumice, UG3 ( $\leq 2$  m) consists of coarse ash dry surge layers, and UG4 (0.55 m) are two grey massive pyroclastic fall deposits with medium to coarse lapilli pumice and enriched in lithics separated by thin coarse ash surge layers, and UG5 (0.3 m) consists of a grey

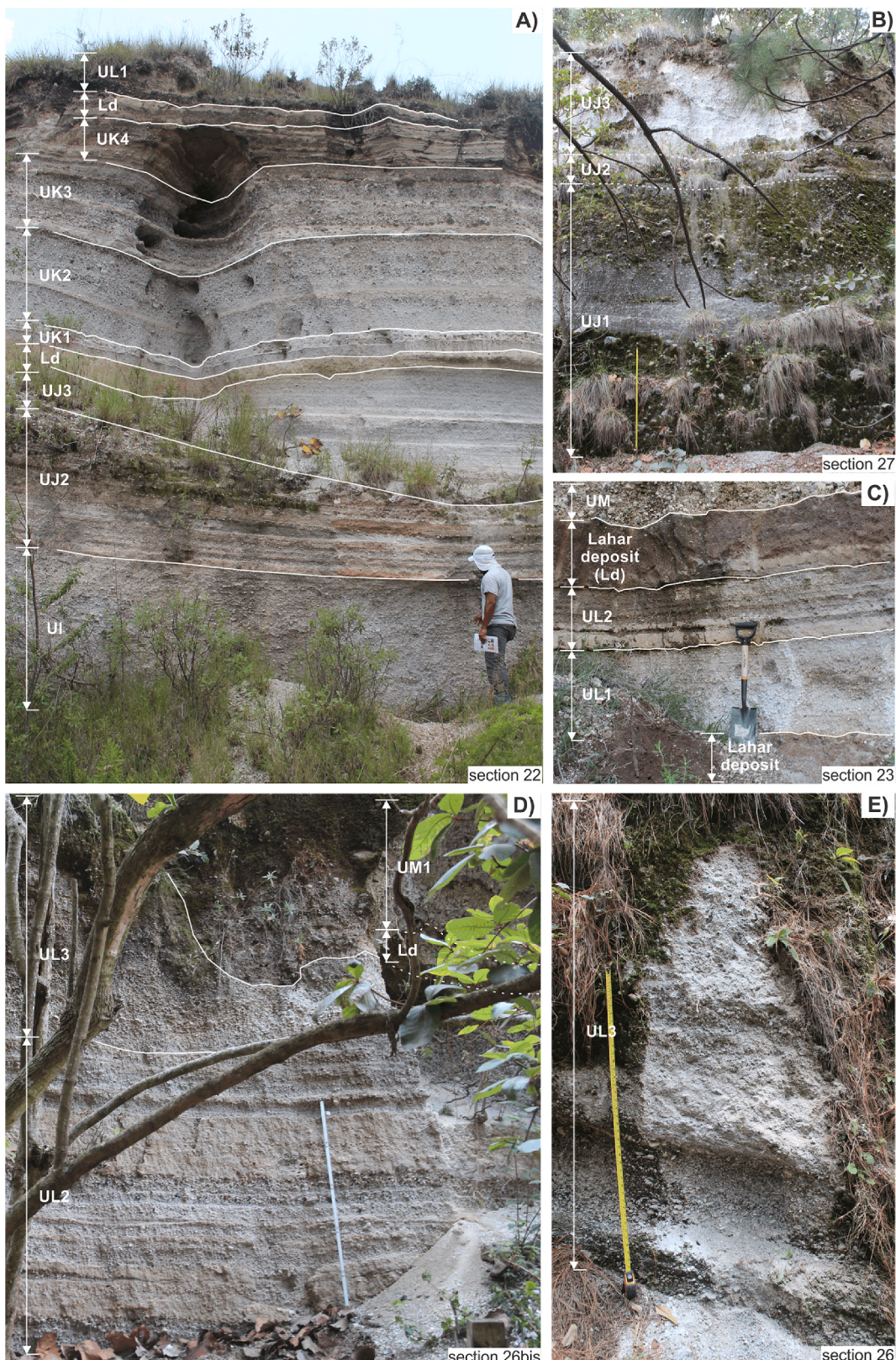


**Fig. 8.** Pictures illustrating the La Primavera I-M pyroclastic units. A) Distal outcrop showing the pyroclastic fall and surges from the I, J2-3, K1-4, and L1 units and subunits. Lahar deposits stands between subunits J3-K1 and K4-L1 with sharp erosive contacts. B) Proximal UJ1 reversely graded pyroclastic flow deposits, UJ2 wet surge deposits, and UJ3 pyroclastic fall. C) Distal outcrop showing the inverse to diffusely stratified pyroclastic fall and wet surges from L1-2 subunits and massive pyroclastic fall deposit from UM. Notice the lahar deposits below UL1 and between UL2 and UM. D) Proximal wet surges and massive pyroclastic fall deposits from L2 and L3 subunits, and massive pyroclastic fall deposit from M1. The L3 and M1 subunits are separated with an erosive contact by a lahar deposit. E) Proximal outcrop showing the pyroclastic flow and fall deposits of L3 subunit. The white continuous and dashed lines mark the approximated boundaries between units. (Color online, 2 column fitting image). (For interpretation of the references to colour in this figure legend, the reader is referred to the Web version of this article.)

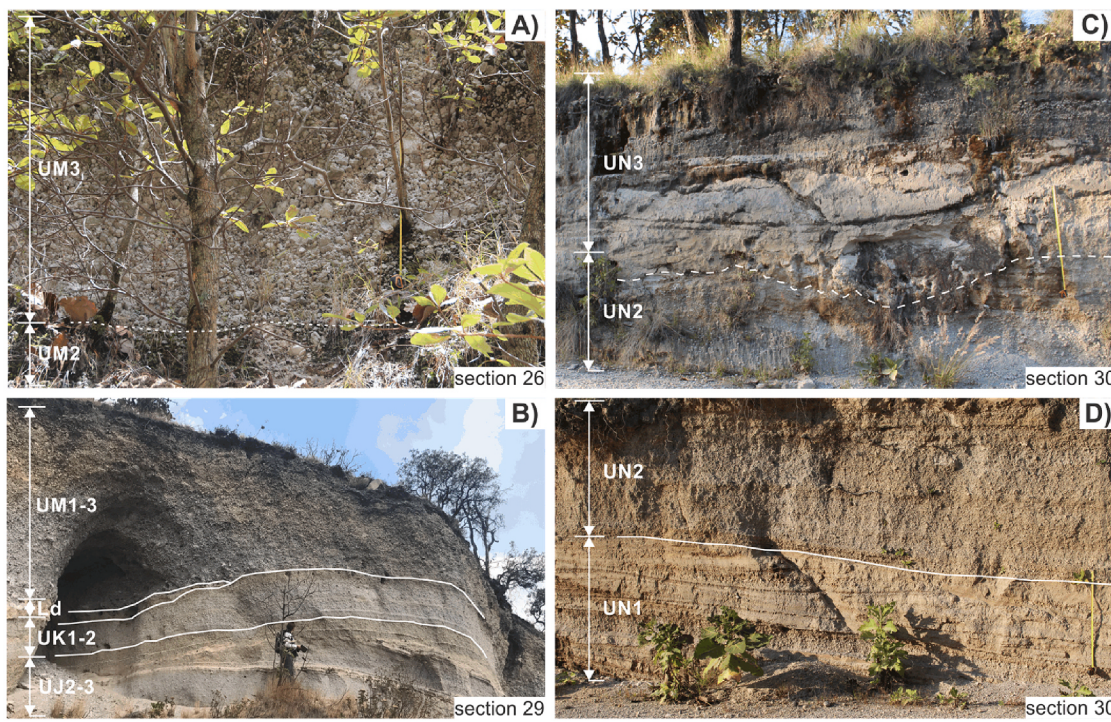


**Fig. 9.** Pictures illustrating proximal outcrops of pyroclastic units J-K and M-N. A) Pyroclastic flow and massive pyroclastic fall deposits from the M2-3 subunits. B) Pyroclastic fall and surge deposits from the J2-3, K1-2 and M1-3 subunits. C and D) Pyroclastic surges and fall deposits, diffuse stratified to massive pyroclastic fall and pyroclastic flow deposits from the N1-3 subunits. The white continuous and dashed lines mark the approximated boundaries between units and subunits. (Color online, 2 column fitting image). (For interpretation of the references to colour in this figure legend, the reader is referred to the Web version of this article.)

diffuse stratified pyroclastic fall made of coarse ash to fine lapilli pumice that toward the top has a thin bed of coarse lapilli pumice and lithics. UG6 (1.9 m) is formed by dry surge layers made of coarse ash to fine lapilli particles rich in obsidian lithics and occasional indurated thin cross-bedded wet surge layers, UG7 (1.4 m) corresponds to a grey reverse to normal graded pyroclastic fall with fine to medium lapilli pumice, and UG8 (1.5 m) consist of coarse ash dry surge layers with an upward decrease in obsidian lithics. The contacts between the different subunits vary from plane sharp to plane sharp to locally erosive. A pumice sample of subunit UG2 collected at section 3 yielded a zircon  $^{230}\text{Th}/\text{U}$  isochron age of  $60.1 \pm 4.0$  ka (Table 1).

#### 6.9. Unit H (UH)

The unit is only exposed in seven stratigraphic sections on the eastern part of the San Miguel volcanic center and on the Puerta dome. UH covers with a sharp erosive contact either UG and a lahar deposit on top of the Puerta dome at sections 14 and 16 (Figs. 6D, 7 A-C, and 10). This unit consists of four sub-units observed in different outcrops. At section 12, UH1 (1.7 m) is a grey, massive, clast-supported, and multiple normal to reverse graded fall deposit made of fine to medium pumice (section 9). UH1bis (0.6 m) is a white pyroclastic flow deposit made of rounded fine to medium pumice and lithics supported by a coarse ash matrix. UH2 (1.4 m) consist of thin cross-bedded wet surge deposits covered by an interbedding of massive, multiple, reverse graded pyroclastic fall deposits with fine to medium lapilli pumice and thin cross-bedded wet surge layers. At section 13, UH3 (4.1 m) consists of a succession of three grey pyroclastic flow deposits made of rounded fine to medium pumice and lithic fragments with some medium-grained to fine-block lithics supported by a coarse ash matrix. UH4 (2 m) is a parallel bedded pyroclastic fall deposit with fine to medium lapilli pumice and thin cross-bedded wet surge deposits. The contacts between subunits are plane sharp to locally erosive. A pumice sample of subunit UH1 collected at section 8 gave a zircon  $^{230}\text{Th}/\text{U}$  isochron age of  $60.3 \pm 0.8$  ka (Table 1).

#### 6.10. Unit I (UI)

This unit was first called E unit by Walker et al. (1981). It lies between units G and J on the Cuesta dome at sections 22 and 23 (Figs. 8A and 10). UI was described in five sections on the Planillas volcanic center and Cuesta dome with variable thickness (0.6–1.8 m). It covers with a undulated sharp contact a paleosol (1.5–2 cm) developed from a lahar deposit on the Cuesta dome (section 22). Here, UI (1.8 m) is a white diffuse stratified pyroclastic fall deposit with fine to medium lapilli pumice. A sample of pumice collected at the base of unit I yielded a zircon  $^{230}\text{Th}/\text{U}$  isochron age of  $58.7 \pm 1.4$  ka (Table 1).

#### 6.11. Unit J (UJ)

This unit was first called unit F by Walker et al. (1981), it is exposed in six sections with variable thickness (1.5–8.9 m). UJ outcrops between a grey lava and UK (close to sections 27 and 27bis), and between UI and UK (section 24) on the northern flank of the Planillas volcanic center, and between UI and UK on the Cuesta dome (sections 22 and 23) (Fig. 8A-B, 9B, and 10). The complete exposure of UJ occurs on the Planillas volcanic center at section 27, here UJ can be divided in three sub-units. UJ1 (7.6 m) is a succession of six grey reversely graded pyroclastic flow deposits with pumice and lithic blocks set in a medium ash matrix. UJ2 (0.3–4 m) is a succession of thick consolidated wet surge layers alternating with grey, clast-supported pyroclastic fall deposits made of coarse ash to medium lapilli pumice. UJ3 (5.1 m) is a grey thick diffuse stratified pyroclastic fall with coarse ash to medium lapilli pumice. The contacts between subunits vary from plane sharp to plane sharp to locally erosive. We did not obtain an absolute age for this unit; however, it is older than unit I ( $58.7 \pm 1.4$  ka) and younger than unit K (see below).

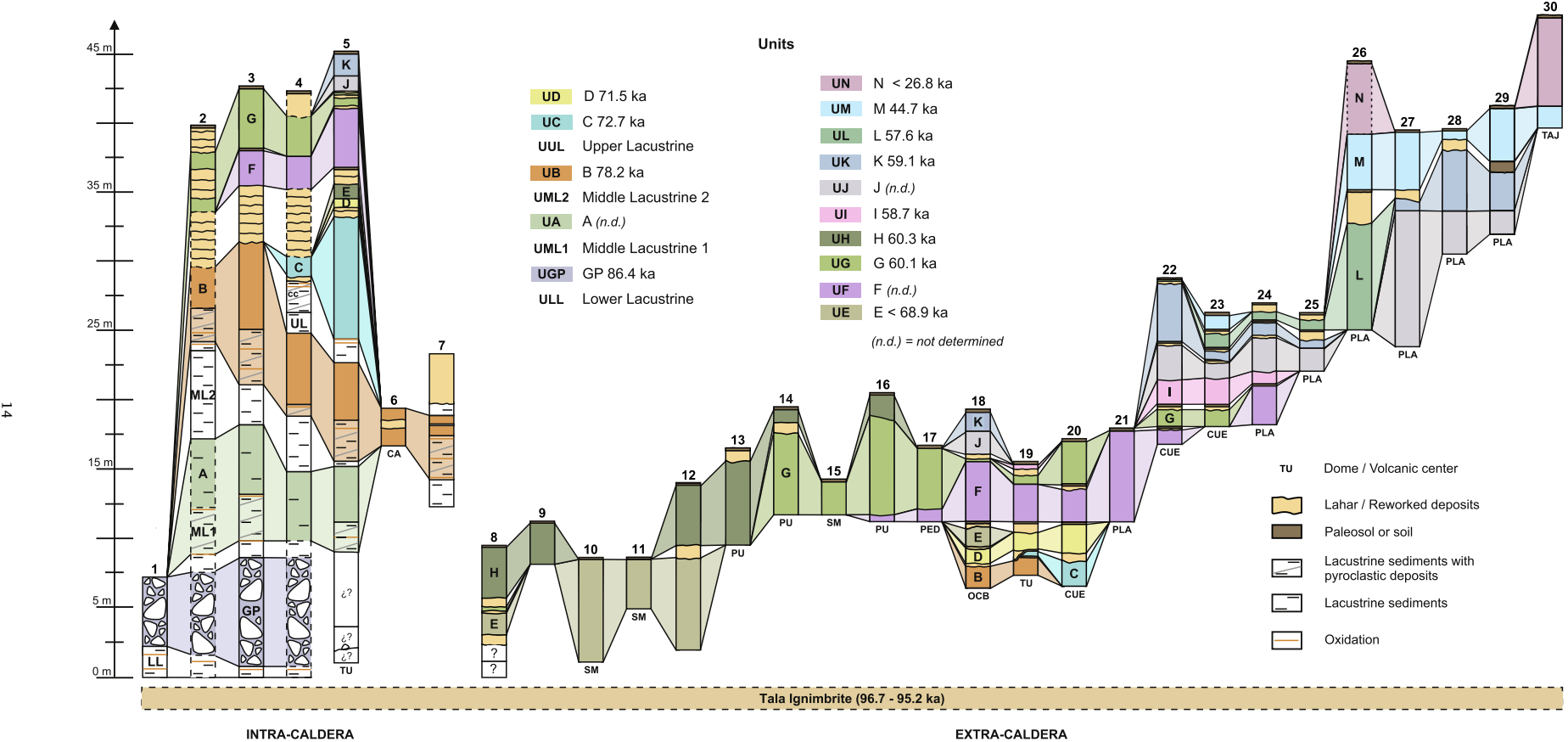


**Fig. 10.** Stratigraphic correlation of the LP pyroclastic deposits and location of the most complete stratigraphic sections. Unit thicknesses to scale except for paleosols. TIU age from Mahood and Drake (1982). Abbreviations from the domes and volcanic centers are the same as in Fig. 1. For column coordinates see Fig. 2 (white circles with numbers) and in the Supplementary material Table 1. (Color online, 2 column fitting image). (For interpretation of the references to colour in this figure legend, the reader is referred to the Web version of this article.)

### 6.12. Unit K (UK)

This unit correlates with unit G of [Walker et al. \(1981\)](#) and fall deposit 2 of [Rivera Olgún \(2016\)](#). It is exposed in eleven sections on top of the Planillas volcanic center and Cuesta, Old Culebreado, and Culebreado domes with a variable thickness (0.35–4.2 m). UK is bracketed between units J and L (sections 23–25) and between units J and M (sections 27–29), and lies atop a 2 cm paleosol on the Cuesta dome (sections 22 and 23) with an undulated sharp contact ([Figs. 8A, 9B and 10](#)). UK can be divided from base to top in four subunits as observed in different outcrops. At section 22 on the Cuesta dome, UK1 (37.5 cm) is a white massive pyroclastic fall deposit with coarse ash to fine lapilli pumice covered by thin fine ash wet surges layers with impact structures, UK2 (1.5 m) is a succession of multiple white massive, reversely graded pyroclastic fall deposits with fine to medium lapilli pumice and abundant lithics, UK3 (1.9 m) is a succession of white massive, pyroclastic fall deposits made of medium to coarse lapilli pumice separated by thin fine ash wet surge layers, and UK4 (0.85 m) that consists of a succession of thick wet surges made of fine ash layers alternating with dry surges made of coarse ash to fine lapilli. The contacts between subunits vary from plane sharp to plane sharp to locally erosive. A pumice sample of subunit K2 collected at section 31 gave a zircon  $^{230}\text{Th}/\text{U}$  isochron age of  $59.1 \pm 3.1$  ka ([Table 1](#)).

### 6.13. Unit L (UL)

This unit was first called H unit by [Walker et al. \(1981\)](#). It occurs in four sections on the Planillas volcanic center and Cuesta dome with thicknesses that vary from 0.8 to 8.3 m. At section 23, UL lies atop a paleosol (3–6 cm thick) developed from a lahar deposit eroding UK on the Cuesta dome ([Fig. 8A,C-E, and 10](#)). This unit can be divided in four subunits. At section 23, UL1 (0.6 m) is a white inverse to diffusely stratified pyroclastic fall made of coarse ash to medium lapilli pumice (L3 Xa). At section 26 bis, UL2 (2.8 m) is a succession of brown thin wet surge layers made of fine ash alternating with fall deposits with coarse ash to fine lapilli pumice and lithics. At section 26, UL3 (5.2 m) is a succession of white massive pyroclastic fall deposits constituted by fine to medium lapilli pumice (L3 Xb and Xc), alternating with grey pyroclastic flow deposits made of fine to medium pumice and lithics set in a coarse ash matrix, and UL4 (2.5 m) is a thick grey to beige pyroclastic flow deposit made of medium to coarse lithics supported by a coarse ash to fine lapilli pumice and lithic matrix with a reworked upper part. The contacts between subunits vary from plane sharp to plane sharp to locally erosive. A pumice sample from subunit L1 collected at section 23 gave a zircon  $^{230}\text{Th}/\text{U}$  isochron age of  $57.6 \pm 5.4$  ka ([Table 1](#)).

### 6.14. Unit M (UM)

This unit correlates with unit J of [Walker et al. \(1981\)](#) and fall deposit 3 of [Rivera Olgún \(2016\)](#). UM is exposed in six sections on top of Planillas and Tajo volcanic centers, and Cuesta dome with a variable thickness (1–4.4 m). It covers with a sharp undulating contact and a paleosol (14 cm thick) developed from a lahar deposit of unit L (section 23), and over unit K on the eastern part of Planillas (section 29) ([Fig. 8C-D, 9 A-B, and 10](#)). At section 26, UM lies beneath UN, where it exhibits the best outcrop that can be divided in three subunits: UM1 (2 m) is a thick white massive pyroclastic fall with medium to coarse lapilli pumice, UM2 (30 cm) is a grey pyroclastic flow deposit with a medium ash matrix, and UM3 (2.1 m) is a thick white massive pyroclastic fall with medium to coarse lapilli pumice. The contacts between subunits varies from erosive to plane sharp. A pumice sampled of unit M collected south of the Tajo volcanic center at section 32 yielded a zircon  $^{230}\text{Th}/\text{U}$  isochron age of  $44.7 \pm 3.2$  ka ([Table 1](#)).

### 6.15. Unit N (UN)

This unit was first called Pir-Tj by [Gómez Álvarez \(2015\)](#). UN is exposed in five sections on the Planillas and Tajo volcanic centers, and on the Cuesta dome. On top of Tajo, UN has a maximum thickness of 7.3 m and covers with a sharp erosive contact unit M (sections 30 and 30bis) ([Fig. 9C-D and 10](#)). Here, UN can be divided from base to top in three subunits: UN1 (2.3 m) consists of grey cross-bedded dry surge layers made of medium to coarse ash alternating with grey pyroclastic fall deposits made of fine to medium lapilli pumice, UN2 (1.6 m) is a thick diffusely stratified to massive pyroclastic fall deposit with fine to medium lapilli pumice. UN3 (>1.9 m) is made of four white pyroclastic flow deposits with rounded fine to medium lapilli pumice and lithic fragments set in a medium ash matrix. The contacts between the sub-units are plane sharp and erosive. We did not obtain an absolute age for this unit; however, it lies between UM ( $44.7 \pm 3.2$  ka) and the Upper Tajo lavas dated between 26.8 and 25.6 ka ([Mahood, 1980; Mahood and Drake, 1982](#)).

## 7. Granulometry and componentry

The Median (Md) and Sorting ( $\sigma\Phi$ ) parameters from thirty samples were calculated to represent the granulometric distribution of main pyroclastic fall and dense PDC deposits ([Fig. 11](#)). The samples A2 Xa, Xc and C1 Xa, Xb are dense PDC deposits with median and sorting parameters that vary from  $-1.25$  to  $-0.6 \Phi$  and from  $2.05$  to  $4.7 \sigma\Phi$ , respectively. The rest of the samples (B–N) are pyroclastic fall deposits with median diameters between  $-3$  and  $3\Phi$ , but subunits K2 and M3, that have median parameters varying from  $-5$  to  $-3.5 \Phi$ , and sorting values between  $1$  and  $2.5 \sigma\Phi$ . Values of the median and sorting parameters are given in the [Supplementary material Table 4](#).

The componentry analysis of those samples indicates that most pyroclastic pumice fall, and dense PDC deposits are composed in order of abundance of pumice, lithics, and crystals ([Fig. 12A](#)). Juvenile fragments are white to grey pumices (vesiculated) and transparent to grey blocky juvenile clasts (non-vesiculated, translucent with glass reflectance). Most units are aphyric to nearly aphyric with less than 3 vol% of phenocrysts counted in the  $1\Phi$  fraction ([Fig. 12B](#)), except for units C and F, that contain between 2 and 11 vol%, respectively. Loose crystals are represented by quartz, sanidine, Fe-hedenbergite and fayalite. Lithic contents are quite variable going from 0.5 to 44 vol% ([Fig. 12C](#)). The main lithics are in order of abundance grey porphyritic lavas with amphibole phenocrysts (andesite), black to red aphanitic tabular lavas (tabular basalt), black porphyritic lavas with white to yellowish crystals, red altered lava fragments, and obsidian. The crystal, blocky juvenile and lithic clast percentages are particularly useful to discern one unit from the other. The percentages calculated are given in the [Supplementary material Table 5](#).

## 8. Discussion

### 8.1. Source of the pyroclastic fall units

The first isopach and isopleth maps of the LP pyroclastic pumice fall succession were presented by [Walker et al. \(1981\)](#). They concluded that six units (D, E, F, G, H and J) had been sourced at Planillas and San Miguel volcanic centers. Based on their descriptions (page 1105, [Fig. 3](#), section 9), we concluded that their six units correspond to our pyroclastic units G, I, J, K, L and M ([Figs. 4 and 10](#)). With this correlation and our new stratigraphic scheme, we present further interpretations on the source of all eruptions described in this work.

For units A–D, the small number of outcrops described impeded the elaboration of representative isopach and isopleth maps. However, we observed that most pyroclastic deposits associated to these units occur south of the Nejahuite composite dome and north of the southern edge of the caldera rim. Therefore, we propose that the source of these

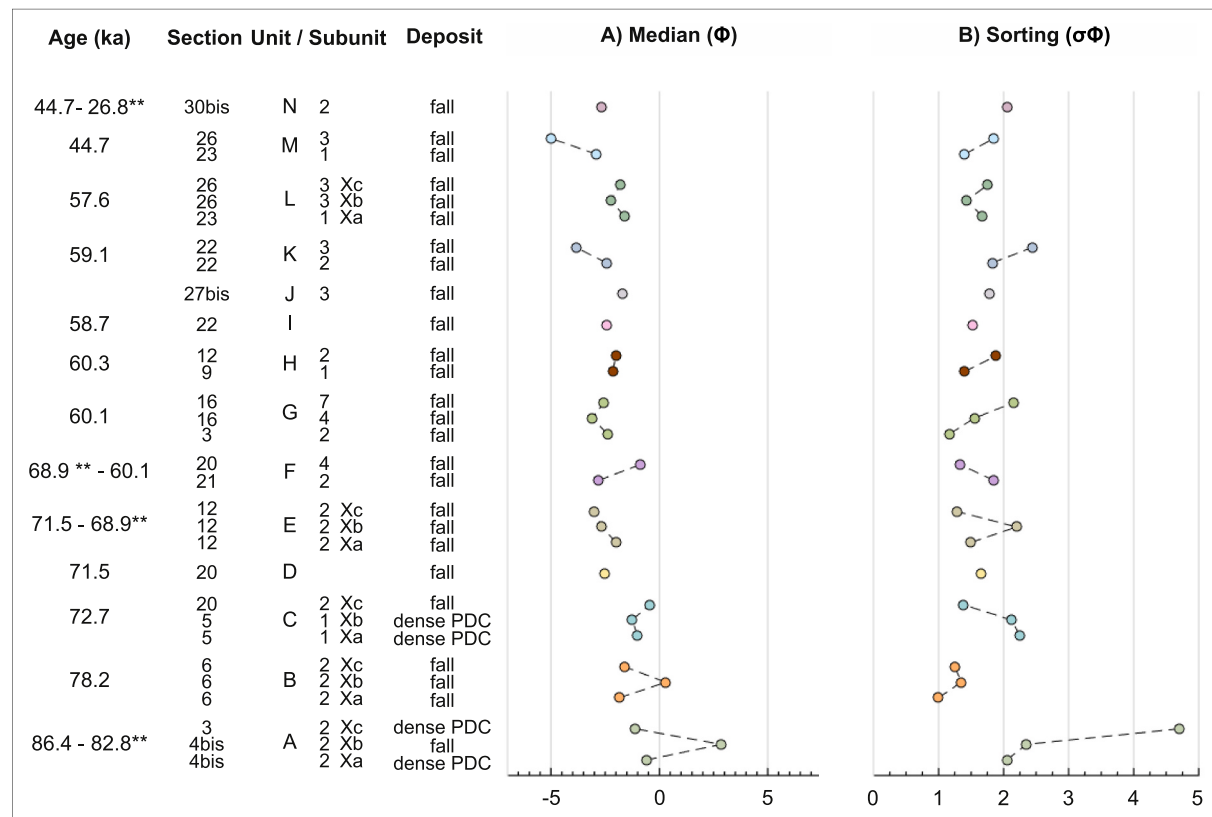


**Fig. 11.** Variation of the median and sorting parameters through the La Primavera stratigraphic column. A) Median ( $\Phi$ ). B) Sorting ( $\sigma\Phi$ ). \*\*Dates taken from Mahood (1980) and Mahood and Drake (1982). (Color online, 2 column fitting image). (For interpretation of the references to colour in this figure legend, the reader is referred to the Web version of this article.)

eruptions may have been located at the Nejahuite composite dome.

Isopleth maps of lithics and isopach maps are proposed for subunits E2, F2, G2, J3, K2, and M1-3 (Figs. 13 and 14). These maps should be considered with caution given the small numbers of outcrops found. Nonetheless, the distribution of the five largest lithic clasts and thickest outcrops from these deposits point out to the possible vent sites.

The pumice fall deposit of sub-unit E2 (71.5–68.9 ka) outcrop on top of the lava from the San Miguel volcanic center with a maximum thickness of 7.4 m. The five largest lithics (22.6 cm) were found close to San Miguel crater indicating this complex as the most likely vent (Figs. 13A and 14A).

The pumice fall F2 (between 68.9 and 60.1 ka) is largely distributed between the Planillas volcanic center and Cerro Alto dome. Nonetheless the thickest deposits (5 m) and largest lithics (6.8 cm) of UF2 were found on the basal part of Planillas indicating this complex as the most likely vent (Figs. 13B and 14B). However, the deposits from this subunit were eroded on the upper flanks of Planillas volcano.

The pumice fall G2 (60.1 ka) is exposed from the southwestern part of San Miguel volcanic center to the Chapulin dome located northeast of the caldera. The G2 largest lithics (4.7 cm) and complete UG pyroclastic sequence were found on the Puerta dome. Most of the UG deposits were eroded on top of San Miguel. The distribution of the pumice fall and the distribution of the associated PDCs point to San Miguel as the possible source (Figs. 13C and 14C).

The deposits of J3 were deposited on top of the Planillas volcanic center and on the Old Culebreado, Culebreado, Tule and Cuesta domes. The thickest deposits (5.1 m) and largest lithics (36 cm) were found close to the Planillas top (Figs. 13D and 14D). The K2 basal pumice fall (59.1 ka) has the same dispersion as unit J3 and the UK2 largest lithics (6.1 cm) were found close to the Planillas top (Figs. 13E and 14E). Most of the UK2 deposits were eroded on top of Planillas. These results indicate that

eruptions J and K were sourced at the Planillas volcanic center.

The deposits of subunits M1-3 (44.7 ka) were found on top of the Planillas and Tajo volcanic centers and Cuesta dome. The thickest deposits (4.4 m) and largest lithics (26.8 cm) of these deposits were found close to the Planillas summit also indicating this volcano as the potential source (Figs. 13F and 14F).

Due to the scarcity of outcrops we were not able to produce isopach and isopleth maps for units H, I, L and N. However, these deposits occur south of La Primavera caldera around the San Miguel, Planillas and Tajo volcanic centers. The UH deposits are dispersed around the San Miguel volcanic center. The deposits of units I (58.7 ka) and L (57.6 ka) are found on top of the Planillas, and on the Old Culebreado, Culebreado and Cuesta domes. Those deposits were partially to completely eroded on top of Planillas. Finally, the thickest deposits (6 m) and largest lithics (7.6 cm) of UN (between 44.7 and 26.8 ka) were found on top of the Tajo volcanic complex. The proposed source of the A-N eruptions is summarized in Fig. 15.

## 8.2. Post-caldera eruptive chronology and evolution

The geological evolution of La Primavera caldera was first described by Mahood (1980, 1981a) and Mahood and Drake (1982). They used the stratigraphic position and K-Ar dates of the domes relative to the Giant Pumice Horizon, and the whole-rock chemistry of rocks to define the evolution of the caldera. At about the same time, Walker et al. (1981) described the pyroclastic stratigraphy and recognized seven post-caldera units named C to J. They defined their possible source and attempted to correlate them to the geological evolution of Mahood and Drake (1982). Nonetheless, the pyroclastic descriptions of Walker et al. (1981) could not be used during our field reconnaissance due to the lack of information of the deposits (e.g. structure, lithic and crystal content) or ages

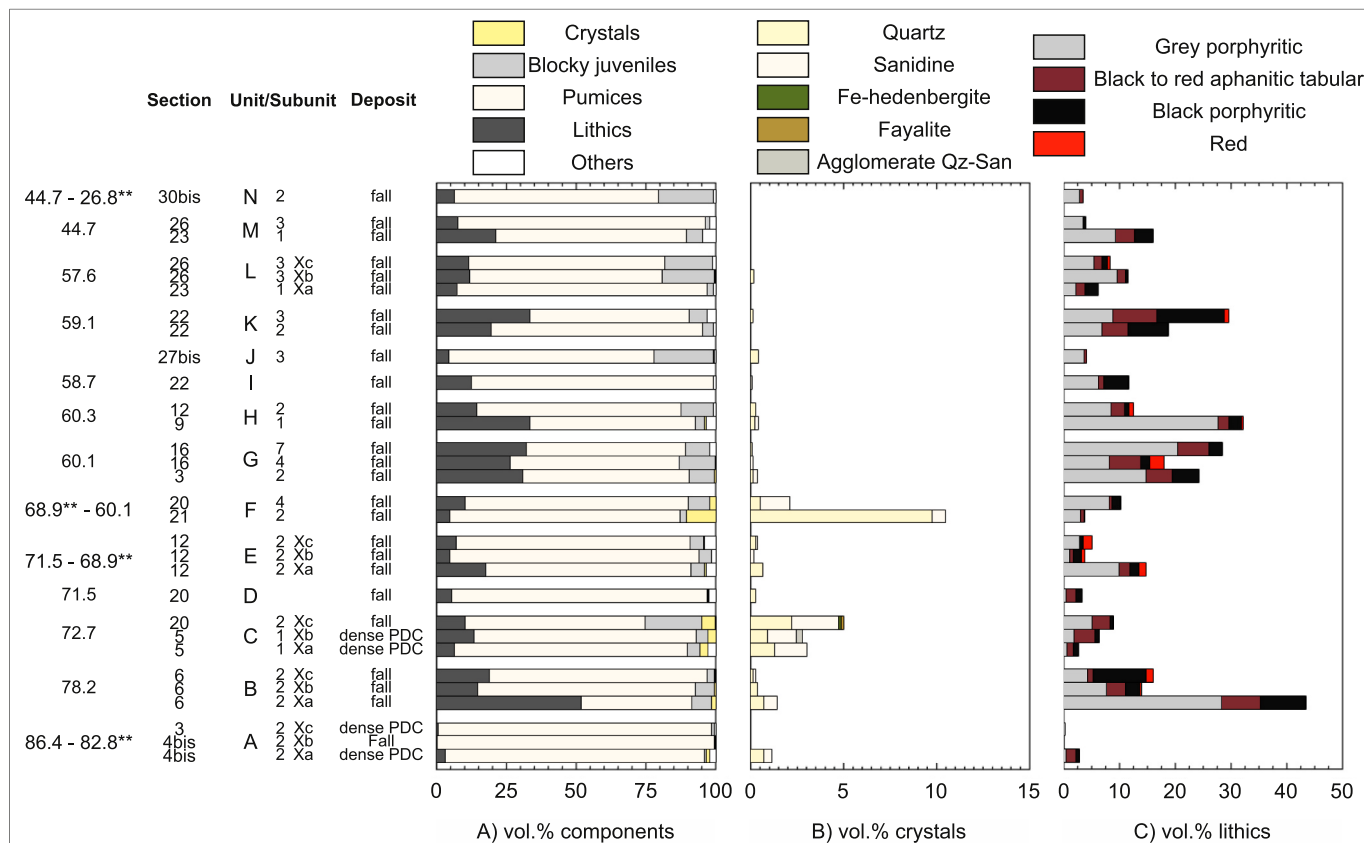


**Fig. 12.** Variation of components through the stratigraphic sequence. A) Lithic, juvenile, and crystal components. B) Crystals. C) Lithics. \*\*Dates from Mahood (1980) and Mahood and Drake (1982). (Color online, 2 column fitting image). (For interpretation of the references to colour in this figure legend, the reader is referred to the Web version of this article.)

of the deposits. In our stratigraphic reconstruction, we recognized at least 14 units (A-N) associated to the same number of eruptions all of them emplaced after the Giant Pumice eruption occurred ca. 86.4 ka. The units of Walker et al. (1981) between brackets would correspond to our units: UG (D), UH (E), UI (F), UJ (G), UK (H) and UL (J). Fig. 16 displays the eruptive chronology of La Primavera caldera that includes the stratigraphic relations between lavas and domes (Mahood and Drake, 1982), and pyroclasts of Walker et al. (1981) and this work. These units were emplaced after the caldera collapse occurred ca. 95 ka and up to 26.8 ka as it will be described next (Fig. 16).

#### 8.2.1. Intra-caldera and caldera ring fault activity

After the collapse of the caldera that occurred ca. 95 ka, several domes were emplaced inside and on the northern and southern parts of the caldera ring fault (Mahood and Drake, 1982). The first eruption that occurred inside the caldera issued lava flows during the initial stages of construction of the Nejahuete composite dome some 93.8 ka (Tinoco Murillo, 2017). At about the same time, other eruptions occurred on the southern part of the caldera ring fault emplacing lavas from the Pilas and Tule domes. The extrusion of lavas from the Nejahuete composite dome marked the beginning of the caldera resurgence. This is in agreement with Mahood (1980) who suggested that magma resurgence began during the first 5 to 10 ka after the caldera formation. After these eruptions, began the lacustrine sedimentation inside the caldera that piled up the Lower Lacustrine unit (ULL). The Nejahuete composite dome reactivated with the subaqueous eruption of the Giant Pumice at about  $86.4 \pm 5.1$  ka (UGP). This very well known eruption produced large pumice blocks ( $\leq 6$  m in diameter) that floated and sank to form the famous Giant Pumice that represents the best stratigraphic marker of La Primavera caldera (Mahood, 1980; Clough et al., 1981). Two hypotheses were proposed to explain its formation: (1) the fragmentation of a

pumiceous carapace of a silicic lava extrusion (Clough et al., 1981) and (2) the fracturing of the upper pumiceous portion of an eruptive column into blocks (Mahood, 1980). These giant pumice blocks were dispersed throughout the lake inside the caldera and on top of the Pilas dome. After this eruption, the sedimentation continued in the lake with the deposition of fine parallel stratified beds of the Middle Lacustrine unit 1 (UML1). Afterwards, Nejahuete reactivated with a series of explosive eruptions (A) that produced pyroclastic falls that were emplaced on the lacustrine environment (UML1) forming ashy lacustrine sediments (UA1). These sediments are partly oxidized suggesting that the lake was shallow to nearly dried at the time of the eruption. This shallow environment could have been due to (1) uplift of the central part of the caldera that caused partial drainage of the lake or (2) infilling of the lake by abundant pyroclastic material that filled and partly dried the lake. In both cases, it seems that the lake became a palustrine environment where oxidation of the most superficial deposits took place. This eruption continued with the dispersion of dilute and dense PDCs and ash fall deposits inside the caldera (UA2), and culminated with the emplacement of an obsidian lava flow (black perlitic) atop the Nejahuete composite dome some 82.8 ka (Mahood, 1980; Mahood and Drake, 1982) and formation of the Cerro Alto dome. Because resurgence continued, Nejahuete and Cerro Alto were subjected to intense mass remobilization with the generation of landslides, lahars, and fluvial deposits. At about the same time (83.6 ka) a new extrusion of magma led to the formation of the Ixtahuatonte (Mahood, 1980; Mahood and Drake, 1982), and Old Culebreando domes that were vented on the southern rim of the caldera.

After these eruptions and during a period of ca. 5 ka the sedimentation in the lake was reestablished allowing the formation of the Middle Lacustrine Unit 2 (UML2). At about  $78.2 \pm 2.8$  ka, a new eruption of Nejahuete (B) formed a small altitude intermittent column that was

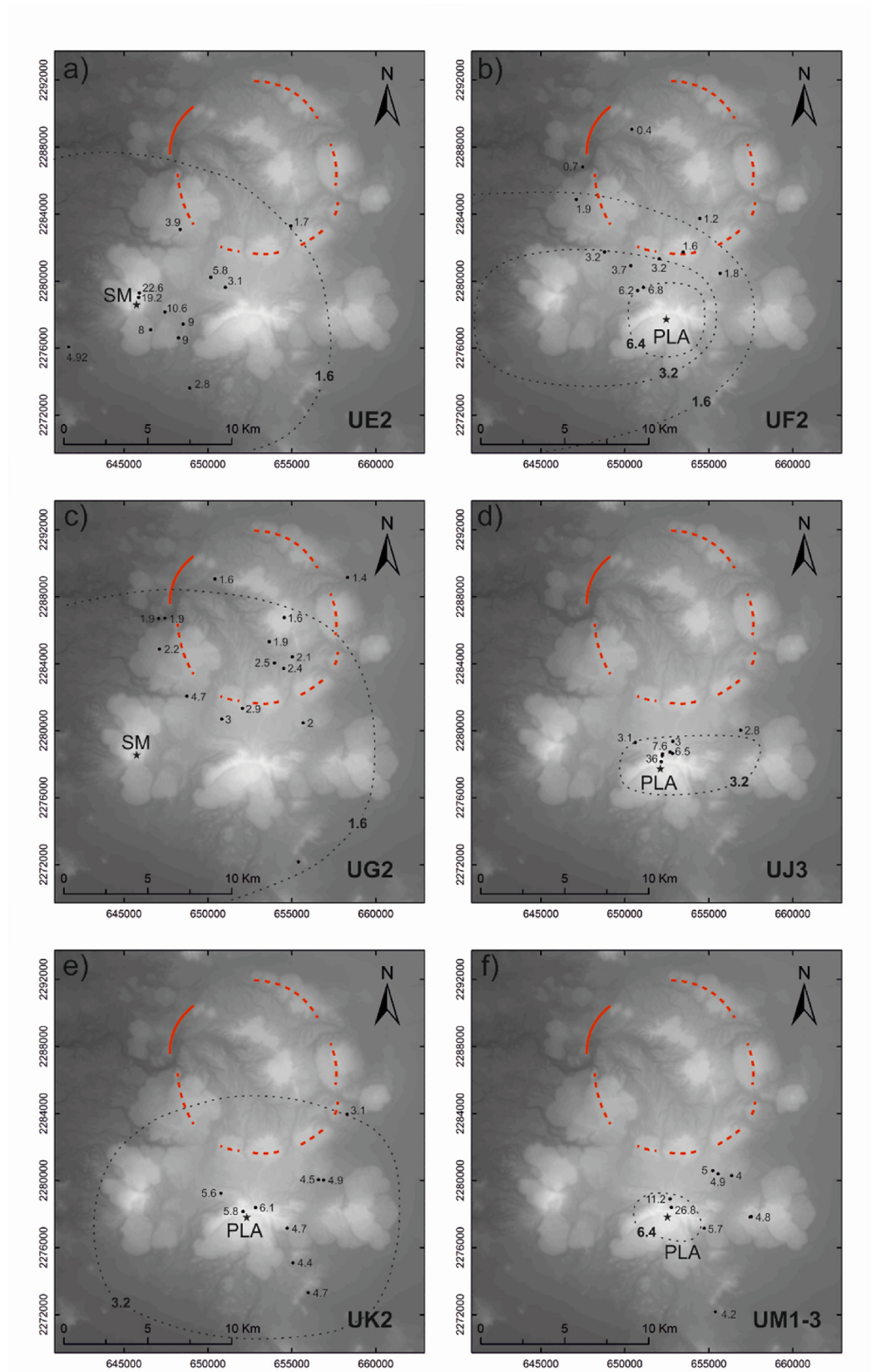


**Fig. 13.** Isopleth maps of units and subunits described in this work (E2, F2, G2, J3, K2 and M1-3) over the DEM of La Primavera caldera. a) UE2. b) UF2. c) UG2. d) UJ3. e) UK2. f) UM1-3. The numbers associated with dots represent the average of the five largest lithic clasts. The dashed lines represent the 6.4, 3.2 and 1.6 lithic isolines from Carey and Sparks (1986). The stars indicate the most likely vents of the pyroclastic fall deposits. (Color online, 2 column fitting image). (For interpretation of the references to colour in this figure legend, the reader is referred to the Web version of this article.)

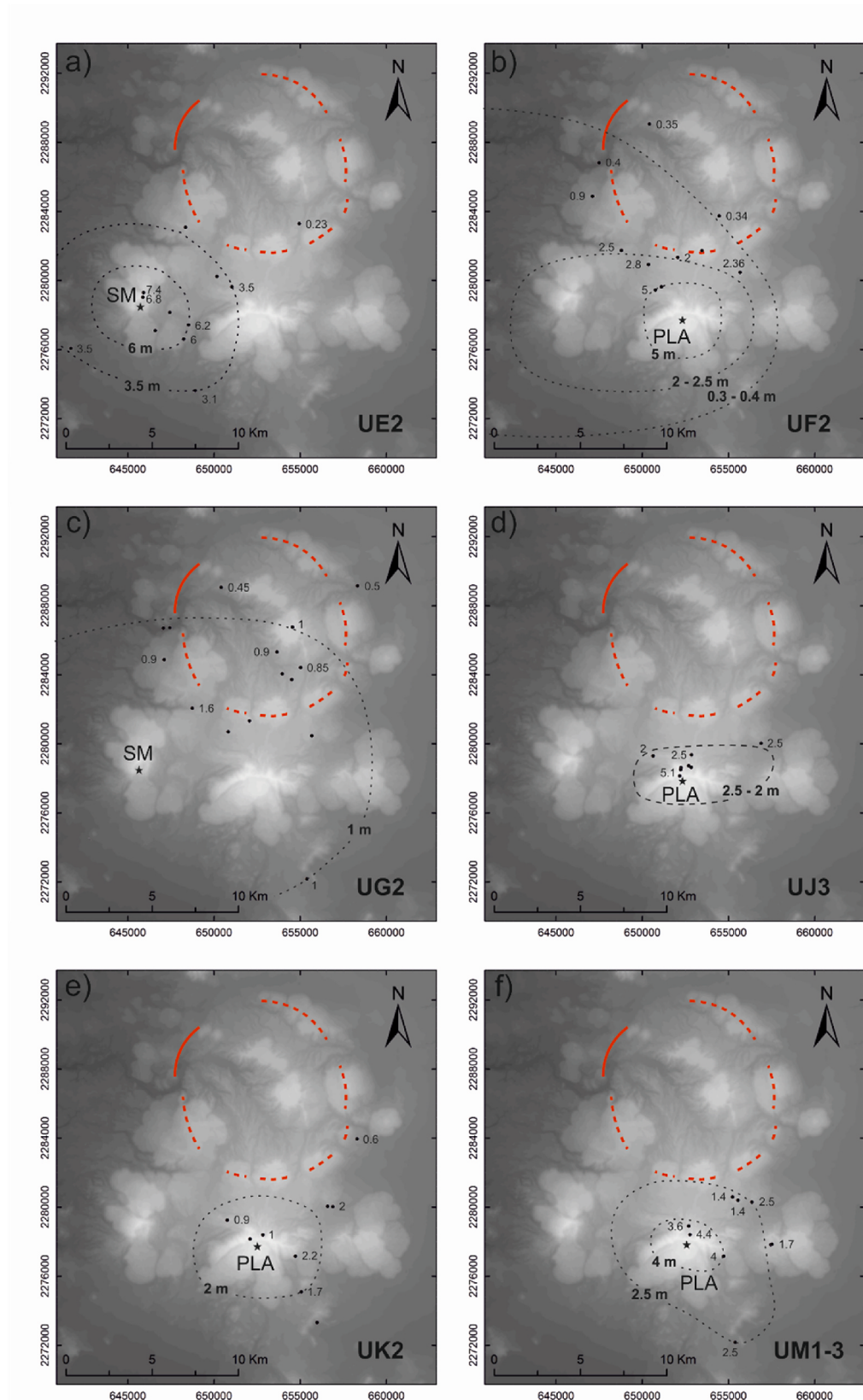


**Fig. 14.** Isopach maps of units and subunits described in this work (E2, F2, G2, J3, K2 and M1-3) over the DEM of La Primavera caldera. a) UE2. b) UF2. c) UG2. d) UJ3. e) UK2. f) UM1-3. The numbers associated with dots represent deposit thickness. The dashed lines show the contour lines of equal thickness. The stars indicate the most likely vents of the pyroclastic fall deposits. (Color online, 2 column fitting image). (For interpretation of the references to colour in this figure legend, the reader is referred to the Web version of this article.)

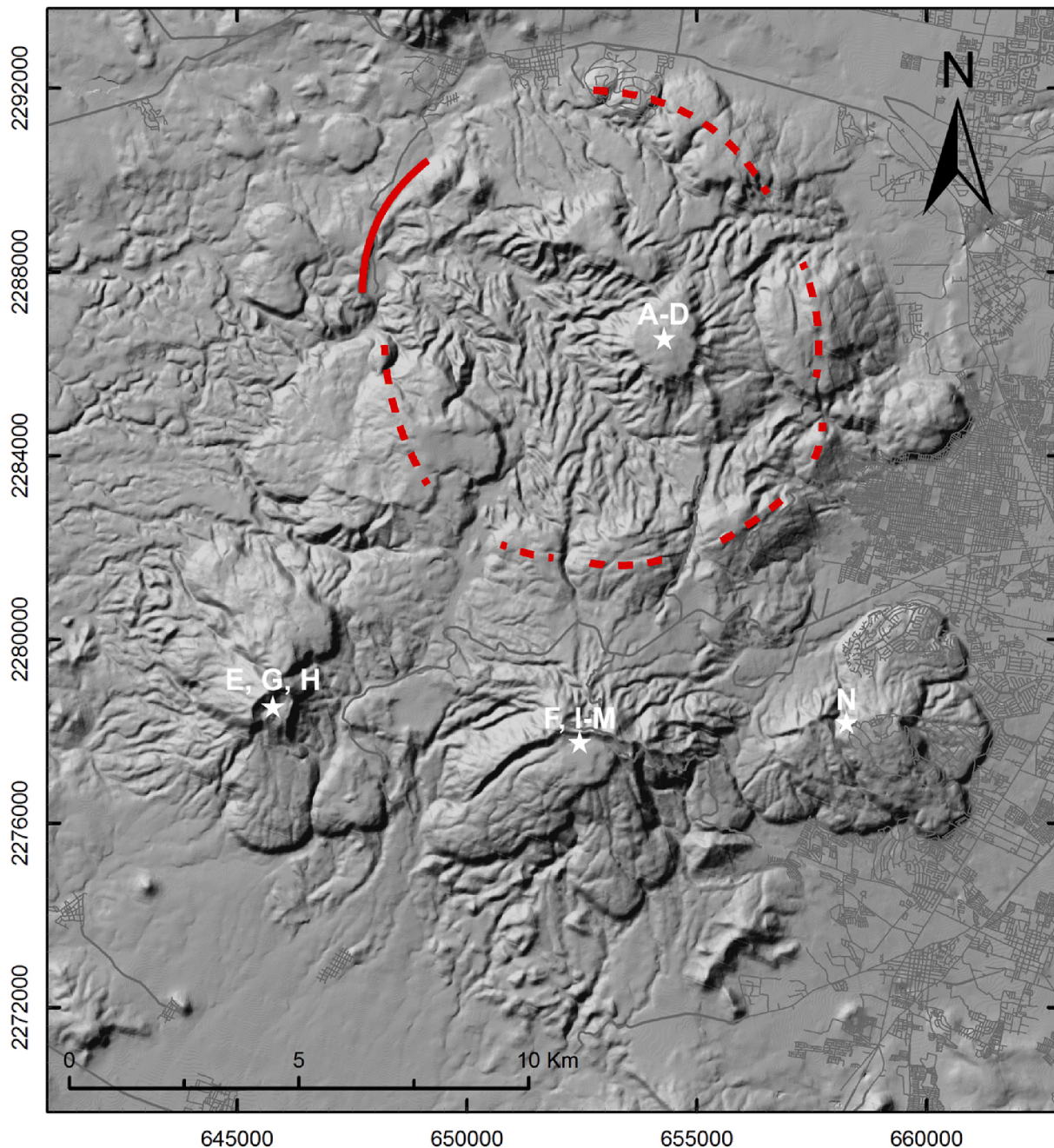


**Fig. 15.** Location of possible vents of the fourteen eruptions occurred between 86.4 and 26.8 ka at La Primavera caldera. The eruptive centers are labeled with white stars and the approximated location of the caldera ring fault with red continuous and dashed lines. (Color online, 2 column fitting image). (For interpretation of the references to colour in this figure legend, the reader is referred to the Web version of this article.)

disrupted by hydromagmatic explosions that dispersed wet dilute PDCs (UB1) between the upper lacustrine beds (UML2). The event increased in intensity over time emplacing a complex succession of wet dilute PDCs, dense PDCs and fallouts enriched in lithics due to erosion of the conduit and vent (UB2). The deposits were confined inside the caldera and the pyroclastic fall from UB2 blanketed the Old Culebreado and Tule domes in the southern part of the caldera rim. The oxidation of the UB2 deposits indicate that they were emplaced in shallow water depths at a time in which resurgence was still underway (78.2 ka). At about 77.2 ka an effusive eruption vented the Culebreado dome on the southern rim of the caldera. Lacustrine sedimentation still continued with the formation of the Upper Lacustrine Unit (UUL) lower part. The LP caldera resurgence ended with the extrusion of the Cerro Colorado lava southeast of Nejahuete some 75.8 ka (Tinoco Murillo, 2017). It vented on a curve

fault called Cerro Colorado dike and Mesa El Nejahuete fault by Mahood (1980) that extends from Cerro Alto to the Tule domes. Shortly thereafter, the Cerro Colorado lava was subjected to intense mass remobilization with the generation of landslides, and fluvialite deposits. Those reworked deposits are interbedded with occasional oxidized lacustrine sediments from the ULL upper part south of Nejahuete. Those results also suggests that the lacustrine sedimentation was about to end.

Some ~2 ka years later reactivation along the southwestern part of the caldera rim extruded the Pedernal lower lavas (73 ka) followed by the extrusion of the Cuesta dome outside of the southeastern border of the caldera (71.3 ka) (Mahood, 1980; Mahood and Drake, 1982). At  $72.7 \pm 2.1$  ka, Nejahuete resumed activity with a sub-Plinian eruption (C) that developed an unstable eruptive column that dispersed several grey dense PDCs inside the caldera (UC1). The eruption continued with

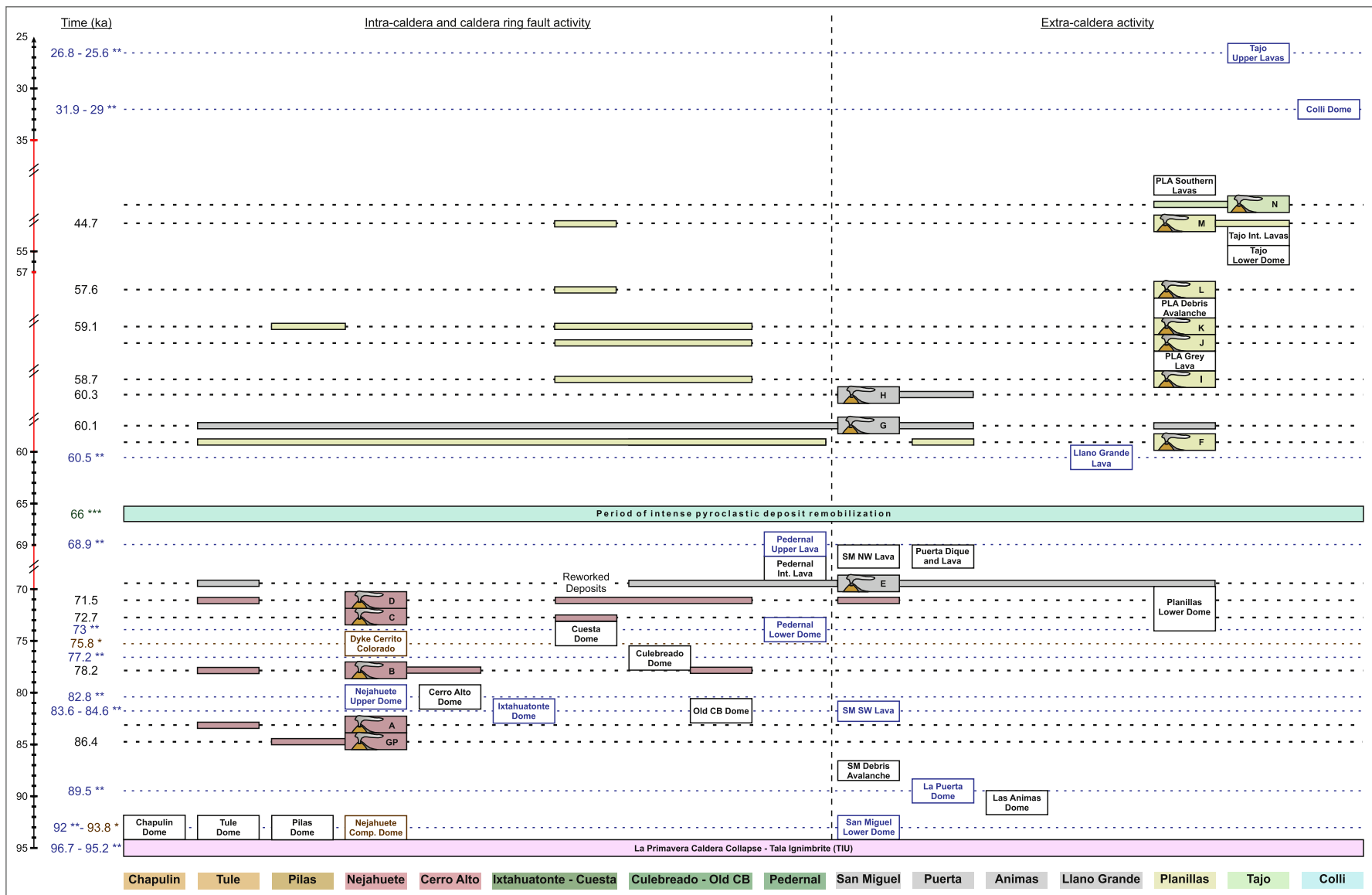


**Fig. 16.** Diagram showing the relation between the post-caldera pyroclastic units of La Primavera caldera (GP to N) with lavas, domes, and volcanic centers. Ages are: A-M units from this work in black; date from Tinoco Murillo (2017) in brown with (\*); and lavas and domes from Mahood (1980) and Mahood and Drake (1982) in blue (\*\*). Warm global event from Kennett et al. (2000) that could be associated to intense remobilization of LP pyroclastic material in green (\*\*). (Color online, 2 column fitting image). (For interpretation of the references to colour in this figure legend, the reader is referred to the Web version of this article.)

the establishment of a more stable eruptive column that deposited a diffuse stratified pyroclastic pumice fall (UC2) inside the caldera and on the Cuesta dome. The last reactivation of Nejahuete (plinian eruption D) occurred  $71.5 \pm 3.0$  ka with the establishment of a vertical eruptive column that dispersed a characteristic white pyroclastic pumice fall with diffuse stratification (UD) inside the caldera and on the Old Culebreado, Culebreado, Tule and Cuesta domes on the southern caldera. After an undefined period of time, San Miguel volcanic center explosively erupted with the establishment of a sub-Plinian column (UE) that was dispersed on the Pedernal lower lavas, Old Culebreado, Culebreado and Tule domes. At about 68.9 ka (Mahood, 1980; Mahood and Drake, 1982), the upper lava of the Pedernal composite dome was extruded along the western caldera rim of La Primavera caldera.

The deposits of eruptions C, D and E were almost completely remobilized by mass wasting processes inside the caldera as attested by metric successions of lahar and fluvialite beds. In order, to remobilize these large volumes of debris from the caldera subaerial outcrops extraordinary rains must have taken place. A global event of increase rainfall around the globe occurred 66 ka ago known as the warm peak of the Marine Isotope Stage 4 recorded in the benthic oxygen isotopic ( $\delta^{18}\text{O}$ ) stratigraphy of the Ocean drilling Program Hole 1017 E east of Point Arguella, California (Kennett et al., 2000). According to these authors this warm peak lasted for about 2 ka, a long period of time that also fit the period of intense mass wasting in La Primavera caldera.

### 8.2.2. Extra-caldera activity

The extra-caldera activity started around 92 and lasted up to 25.6 ka. It mostly concentrated along a NW-SE fault south of the caldera ring-fault with the formation of the San Miguel, Planillas and Tajo volcanic centers, the Puerta and Animas domes and Llano Grande lava (Mahood, 1980). This activity began almost contemporaneously with intra-caldera activity centered at the Nejahuete composite dome.

**8.2.2.1. San Miguel volcanic center, the animas and puerta domes (92–60.3 ka).** The extra-caldera activity began 92 ka with the emission of lava flows that formed the San Miguel volcanic center (Mahood and Drake, 1982). After a few thousand years, effusive activity on the northern flank of San Miguel led to the formation of the Animas dome and to the subsequent emission of the La Puerta dome (89.5 ka; Mahood, 1980; Mahood and Drake, 1982).

Between 92 and 84.4 ka, the southern flank of San Miguel was destroyed by a flank collapse that emplaced a debris avalanche to the south. Then at about 84.4 ka (Mahood, 1980; Mahood and Drake, 1982), reactivation of San Miguel erupted a lava flow inside this collapsed scar. The activity of San Miguel resumed between 71.5 and 68.9 ka with a sub-Plinian eruption (E) that formed a fluctuating and partially collapsing eruptive column that was interrupted several times by contemporaneous basal hydromagmatic explosions that dispersed a sequence of dilute and dense PDCs alternating with pumice fallouts (UE1). As the eruption continued the eruptive column dispersed thick multiple reversely graded pumice fallouts alternating with a few dilute PDCs (UE2). The abundance of blocky juvenile clasts and pumice with small elongated vesicles and wet surge deposits suggests that magma-water interaction played an important role during magma fragmentation. This type of deposits suggest that this activity of San Miguel behave as a sub-Plinian eruption as it was described at Vesuvius (Cioni et al., 2011). The deposits from this eruption were found around San Miguel, and as far as the Cuesta dome, as reworked deposits. Renewed activity of the Puerta dome emitted an obsidian dike and a lava flow on its eastern flank. Then, San Miguel was reactivated with the emission of a lava flow to the northwest followed by the UFplinian eruption from Planillas that dispersed a thick pumice fall to the north. Right after this eruption ( $60.1 \pm 4.0$  ka), San Miguel resumed activity with another fluctuating eruptive column marked by repeated collapses of the external colder parts producing dilute PDCs (UG1). The same

sequence of events emplaced a multiple normal to reversely graded fallout (UG2), dilute PDCs (UG3), two massive fallouts rich in lithics attesting for erosion of the conduit and vent separated by dilute PDCs (UG4), and a diffusely stratified fallout (UG5). Erosion of the conduit continued whereas external parts of the column repeatedly collapsed generating dilute PDCs alternating with occasional hydromagmatic explosions that dispersed wet dilute PDCs (UG6). Afterwards, the eruption was able to sustain a more stable column that dispersed a reverse to normal grading fallout with still visible signs of vent and conduit erosion (UG7) that allowed the external parts of the column to collapse generating further dilute PDCs (UG8). The complex pumice fall deposits of this eruption blanketed as far as the Planillas debris avalanche to the south and Cerro Alto and Chapulin domes to the north. At about  $60.3 \pm 0.8$  ka, San Miguel resumed activity with a sub-Plinian eruption (H). This eruption formed an unstable eruptive column that generated a multiple normal to reverse graded pyroclastic fall deposit and several dense white PDCs (UH1) that traveled  $\approx 3.2$  km to the south. The eruptive column was disrupted by hydromagmatic explosions that emplaced pumice fallouts and wet dilute PDCs to the western part of the Llano Grande lava (UH2) followed by dense PDCs (UH3) that reached the Puerta dome to the east, and pyroclastic falls alternating with wet dilute PDCs (UH4) found on the southern part of the Puerta dome. The last event in the San Miguel area occurred 60.5 ka through the emission of the Llano Grande lava that was dispersed to the southeast (Mahood and Drake, 1982).

**8.2.2.2. Planillas volcanic center (>71.5–44.7 ka).** There is no age for the lavas that began the construction of the Planillas volcanic center  $\approx 7.1$  km to the east of San Miguel volcano. The activity of Planillas started with the emission of lava flows that ended with a black obsidian lava. These lavas were covered by the pyroclastic fall (E) vented at San Miguel. Between 68.9 and 60.1 ka, Planillas volcano explosively reawakened (F) with the establishment of a small eruptive column that dispersed a pumice fall (UF1). Then, the eruption intensified forming a quite stable column that dispersed to the north a thick diffuse stratified pumice fall (UF2) followed by the partial collapse of the eruptive column that emplaced a dense PDC (UF3). The eruption ended with hydromagmatic explosions that disturbed the eruptive column and dispersed pumice falls interlayered with wet dilute PDCs (UF4-5). A few hundred to thousand of years after as attested by the formation of a thin paleosol, San Miguel volcano erupted again (G occurred  $60.1 \pm 4.0$  ka) dispersing pumice falls on the products of the eruption F from Planillas.

Explosive reactivation of Planillas occurred at  $58.7 \pm 1.4$  ka with the establishment of a Plinian eruption (I) that developed an eruptive column that dispersed a diffuse stratified pumice fall (UI) to the north. The activity continued with the emission of a grey lava on its northern flank. Sometime after, Planillas renewed explosive activity (J) with a low fountain of pyroclasts that poured a series of dense PDC (UJ1) toward its northern flank. Then a sub-Plinian column established ensuing by hydromagmatic explosions producing an interlayered set of wet dilute PDCs and pumice falls (UJ2) and a diffusely stratified pumice falls (UJ3). After hundreds to a few thousand years as attested by the formation of a thin paleosol, Planillas volcano ( $59.1 \pm 3.1$  ka) reactivated with another sub-Plinian eruption (K). The eruption began with the formation of an eruptive column that was disturbed by basal hydromagmatic explosions that emplaced a set of ash falls and wet dilute PDCs (UK1). The energy of the eruption column gained and lost strength resulting in a pumice fall with repeated inverse to normal grading parts (UK2). As the eruptive column continued it was disturbed by hydromagmatic explosions that emplaced pumice falls enriched in lithics interlayered with wet dilute PDCs (UK3). Towards the end of eruption K, hydromagmatic explosions interrupted the eruptive column producing its collapsed issuing a complex set of wet and dry dilute PDCs (UK4). After this eruption a major event in the evolution of Planillas volcano occurred with the collapse of its southern flanks that generated a debris avalanche toward the south.

The event completely changed the morphology of Planillas with a semiconical edifice on its northern half and a huge amphitheater open to the south.

At about  $57.6 \pm 5.4$  ka Planillas volcano reactivated again with another sub-Plinian type eruption (L). At the beginning, the eruptive column dispersed an inverse to diffusely stratified pumice fall poor in lithics (UL1) that was then disturbed by hydromagmatic explosions dispersing a succession of wet dilute PDCs interlayered with pumice falls enriched in lithics (UL2). As the eruption continued external parts of the eruptive column collapsed issuing dense PDCs that interlayered with pyroclastic falls (UL3). The eruption ended with the collapse of the column producing a thick dense PDC (UL4).

The last explosive eruption of Planillas volcano occurred  $44.7 \pm 3.2$  ka through the development of a Plinian eruption (M). This eruptive column emitted a thick massive pumice fall (UM1) toward the Cuesta dome to the north and widely to the south. External parts of the eruptive column collapsed generating a small PDC (UM2) and ended with the emission of a massive pumice fall (UM3) that blanketed the volcano's top, Tajo volcano, and the Cuesta dome. Activity of Planillas continued later on with the emission of several lava flows that filled the amphitheater collapse up to reach the present morphology of the volcano.

**8.2.2.3. Tajo volcanic complex (>44.7–26.8 ka).** The Tajo volcanic center began its activity 5.5 km to the east of Planillas along the NW-SE southern fault. Its construction began with the emission of lavas flows to the west and to the east of the vent. Unfortunately, there is no age of these lavas, however, they are older than the pyroclastic deposits of eruption M of Planillas ( $44.7 \pm 3.2$  ka), that cover them. The only explosive activity that we recorded at Tajo produced a sub-Plinian eruption (N) that dispersed pumice falls on top of Cuesta dome and Planillas volcano and emplaced dense and dilute PDCs in proximal locations of the vent (UN). The final activity of Tajo occurred 26.8–25.6 ka (Mahood and Drake, 1982) with another effusive eruption that issued lava flows to the north and south.

## 9. Conclusions

The reconstruction of the post-caldera stratigraphy of La Primavera caldera supported by fieldwork and  $^{230}\text{Th}/\text{U}$  dates indicate that at least fourteen eruptions occurred after the Giant Pumice eruption between 86.4 and 26.8 ka. Based on the structural and textural characteristics of their deposits these eruptions were classified either as sub-Plinian (A, B, E, G, H, J, K, L and N) or Plinian type events (C, D, F, I and M) suggesting that magma water interaction was frequently present during the evolution of the caldera. The deposit distributions, largest lithics and ages suggest four possible sources for these explosive eruptions: intra-caldera activity was focused at Nejahuete (A-D) whereas extra-caldera activity occurred at San Miguel (E, G and H), Planillas (F, I, J, K, L and M) and Tajo (N) volcanic centers.

Intra-caldera activity was centered at Nejahuete composite dome between 93.8 and 71.5 ka that produced five explosive eruptions that interrupted the lacustrine sedimentation and sometimes infilled the lake to a palustrine environment with oxidizing conditions. During this period of ca. 20 ka, caldera resurgence occurred lasting up to  $\sim 75.8$  ka. Extra-caldera activity from San Miguel, Planillas and Tajo volcanic centers occurred between 92 and 26.8 ka, along a NW-SE fault south of the caldera ring-fault. These events generated ten explosive eruptions between 71.5 and 26.8 ka (E-N). The last explosive post-caldera eruption (N) occurred at Tajo volcano between 44.7 and 26.8 ka.

Our new  $^{230}\text{Th}/\text{U}$  geochronology provided new lights on the evolution of the La Primavera caldera. However, further stratigraphy and chronology of the deposits is still needed to further define the timing between effusive and pyroclastic eruptions of La Primavera.

## 10. Author statement

Delphine R. N. Sourisseau: Conceptualization, Methodology, Investigation, Formal analysis, Writing – Original Draft, Writing – Review & Editing, Visualization. José L. Macías: Conceptualization, Investigation, Writing – Review & Editing, Supervision, Funding acquisition. Felipe Garcia Tenorio: Investigation, Writing – Review & Editing. Denis Ramón Avellán: Investigation, Writing – Review & Editing. Ricardo Saucedo Girón: Investigation, Writing – Review & Editing. Juan P. Bernal: Formal analysis, Resources. José L. Arce Saldaña: Writing – Review & Editing. Zareth Tinoco Murillo: Investigation, Resources.

## Declaration of competing interest

The authors declare that they have no known competing financial interests or personal relationships that could have appeared to influence the work reported in this paper.

## Acknowledgments

This work was supported by the CONACyT Doctoral Grant 591186 and by the CONACyT-SENER Grant 207032 of the Centro Mexicano de Innovación en Energía Geotérmica (CeMIE-Geo) project P15 to J.L. Macías. We are thankful to F. Mendiola, G. Cisneros and O. Lopez for their technical support. Special thanks to all the Geophysics Institute Michoacán unit for their support and help to carry this work. Thank you to my friends F. Tapia Vázquez, Z.S. Tinoco Murillo and E. Pacheco for their help in the field. Thanks to the director of the Cielo Country Club who permitted us to describe the deposits lying on the Tajo volcanic center.

## Appendix A. Supplementary data

Supplementary data to this article can be found online at <https://doi.org/10.1016/j.jsames.2020.102747>.

## References

- Avellán, D.R., Macías, J.L., Layer, P.W., Cisneros, G., Sánchez-Núñez, J.M., Gómez-Vasconcelos, M.G., Osorio-Ocampo, S., 2019. Geology of the late pliocene–pleistocene Acoculco caldera complex, eastern Trans-Mexican volcanic Belt (méxico). J. Maps 15 (2), 8–18. <https://doi.org/10.1080/17445647.2018.1531075>.
- Bailey, R.A., Dalrymple, G.B., Lanphere, M.A., 1976. Volcanism, structure, and geochronology of long valley Caldera, Mono county, California. J. Geophys. Res. 81 (5), 725–744. <https://doi.org/10.1029/JB081i005p00725>.
- Bernal, J.P., Solari, L.A., Gómez-Tuena, A., Ortega-Obregón, C., Mori, L., Vega-González, M., Espinosa-Arbeláez, D.G., 2014. In-situ  $^{230}\text{Th}/\text{U}$  dating of Quaternary zircons using LA-MCICPMS. Quat. Geochronol. 23, 46–55. <https://doi.org/10.1016/j.quageo.2014.06.003>.
- Carey, S., Sparks, R.S., 1986. Quantitative models of the fallout and dispersal of tephra from volcanic eruption columns. Bull. Volcanol. 48 (2–3), 109–125. <https://doi.org/10.1007/BF01046546>.
- Cheng, H., Edwards, R.L., Shen, C.C., Polyak, V.J., Asmerom, Y., Woodhead, J., Wang, X., 2013. Improvements in  $^{230}\text{Th}$  dating,  $^{230}\text{Th}$  and  $^{234}\text{U}$  half-life values, and U–Th isotopic measurements by multi-collector inductively coupled plasma mass spectrometry. Earth Planet Sci. Lett. 371, 82–91. <https://doi.org/10.1016/j.epsl.2013.04.006>.
- Cioni, R., Bertagnini, A., Andronico, D., Cole, P.D., Mundula, F.I., 2011. The 512 AD eruption of Vesuvius: complex dynamics of a small scale subplinian event. Bull. Volcanol. 73 (7), 789–810. <https://doi.org/10.1007/s00445-011-0454-3>.
- Clough, B.J., Wright, J.V., Walker, G.P.L., 1981. An unusual bed of giant pumice in Mexico. Nature, 289(5793) 49. <https://doi.org/10.1038/289049a0>.
- Cole, J.W., Spinks, K.D., 2009. Caldera volcanism and rift structure in the Taupo volcanic zone, New Zealand. Geol. Soc. Lond. Spec. Publ. 327 (1), 9–29. <https://doi.org/10.1144/SP327.2>.
- Cruz Lara, A.U., 2015. Evolución del Domo San Miguel, Campo Volcánico La Primavera, Jalisco, México. Estudio de Estratigrafía y Géoquímica.
- DeMets, C., Stein, S., 1990. Present-day kinematics of the Rivera plate and implications for tectonics in southwestern Mexico. J. Geophys. Res.: Solid Earth 95 (B13), 21931–21948. <https://doi.org/10.1029/JB095iB13p21931>.
- Di Paola, G.M., 1974. Volcanology and petrology of Nisyros island (dodecanese, Greece). Bull. Volcanol. 38 (3), 944–987. <https://doi.org/10.1007/BF02597100>.
- Ferrari, L., Conticelli, S., Vaggelli, G., Petrone, C.M., Manetti, P., 2000a. Late Miocene volcanism and intra-arc tectonics during the early development of the Trans-Mexican

- Volcanic Belt. *Tectonophysics* 318 (1–4), 161–185. [https://doi.org/10.1016/S0040-1951\(99\)00310-8](https://doi.org/10.1016/S0040-1951(99)00310-8).
- Ferrari, L., Rosas-Elguera, J., Delgado-Granados, H., Aguirre-Díaz, G., Stock, J.M., 2000b. Late Miocene to Quaternary extension at the northern boundary of the Jalisco block, western Mexico: the Tepic-Zacoalco rift revised. *Geol. Soc. Am. Spec. Pap.* 334, 42–64.
- Ferrari, L., López-Martínez, M., Rosas-Elguera, J., 2002. Ignimbrite flare-up and deformation in the southern Sierra Madre Occidental, western Mexico: implications for the late subduction history of the Farallon plate. *Tectonics* 21 (4). <https://doi.org/10.1029/2001TC001302>, 17–1.
- Gilbert, C.M., Carmichael, I.S., Mahood, G.A., 1985. Volcanic stratigraphy of the Guadalajara area, Mexico. *Geofisc. Int.* 24 (1).
- Gómez Álvarez, F., 2015. Análisis petrológico de los domos Tajo y Colli e implicaciones en el potencial geotérmico del Complejo Volcánico La Primavera (CVLP), Jalisco. <http://nинive.uaslp.mx/xmlui/handle/1/4095>.
- Hon, K., Lipman, P.W., 1989. Western San Juan caldera complex. *New Mexico Bur. Mines and Miner. Resour. Mem.* 46, 350–380.
- Inman, D.L., 1952. Measures for describing the size distribution of sediments. *J. Sediment. Res.* 22 (3), 125–145. <https://doi.org/10.1306/D42694DB-2B26-11D7-8648000102C1865D>.
- Jaffey, A.H., Flynn, K.F., Glendenin, L.E., Bentley, W.T., Essling, A.M., 1971. Precision measurement of half-lives and specific activities of U 235 and U 238. *Phys. Rev. C* 4 (5), 1889. <https://doi.org/10.1103/PhysRevC.4.1889>.
- Jordan, N.J., Rotolo, S.G., Williams, R., Speranza, F., McIntosh, W.C., Branney, M.J., Scaillet, S., 2018. Explosive eruptive history of Pantelleria, Italy: repeated caldera collapse and ignimbrite emplacement at a peralkaline volcano. *J. Volcanol. Geoth. Res.* 349, 47–73. <https://doi.org/10.1016/j.jvolgeores.2017.09.013>.
- Kennedy, B., Wilcock, J., Stix, J., 2012. Caldera resurgence during magma replenishment and rejuvenation at Valles and Lake City calderas. *Bull. Volcanol.* 74 (8), 1833–1847. <https://doi.org/10.1007/s00445-012-0641-x>.
- Kennett, J.P., Roark, E.B., Cannariato, K.G., Ingram, B.L., Tada, R., 2000. Latest quaternary paleoclimatic and radiocarbon chronology, hole 1017E, southern California MARGIN-1. In: Ocean Drill. Program, Sci. Results, vol. 167, pp. 249–254.
- Luhr, J.F., Lazar, P., 1985. The southern Guadalajara volcanic chain, Jalisco, Mexico. *Geofisc. Int.* 24 (4).
- Luhr, J.F., Nelson, S.A., Allan, J.F., Carmichael, I.S., 1985. Active rifting in southwestern Mexico: Manifestations of an incipient eastward spreading-ridge jump. *Geology* 13 (1), 54–57. [https://doi.org/10.1130/0091-7613\(1985\)13<54:ARISMM>2.0.CO;2](https://doi.org/10.1130/0091-7613(1985)13<54:ARISMM>2.0.CO;2).
- Mahood, G.A., 1977. A preliminary report on the comenditic dome and ash flow complex of Sierra La Primavera, Jalisco. *Rev. Mex. Ciencias Geol.* 1 (2), 177–190.
- Mahood, G.A., Drake, R.E., 1982. K-Ar dating young rhyolitic rocks: a case study of the Sierra La Primavera, Jalisco, Mexico. *Geol. Soc. Am. Bull.* 93 (12), 1232–1241. [https://doi.org/10.1130/0016-7606\(1982\)93<1232:KDYRRA>2.0.CO;2](https://doi.org/10.1130/0016-7606(1982)93<1232:KDYRRA>2.0.CO;2).
- Mahood, G.A., 1981a. A summary of the geology and petrology of the Sierra La Primavera, Jalisco, Mexico. *J. Geophys. Res.: Solid Earth* 86 (B11), 10137–10152. <https://doi.org/10.1029/JB086iB11p10137>.
- Mahood, G.A., 1981b. Chemical evolution of a Pleistocene rhyolitic center: Sierra la Primavera, Jalisco, Mexico. *Contrib. Mineral. Petrol.* 77 (2), 129–149. <https://doi.org/10.1007/BF00636517>.
- Mahood, G.A., 1980. Geological evolution of a Pleistocene rhyolitic center—sierra la Primavera, Jalisco, Mexico. *J. Volcanol. Geoth. Res.* 8 (2–4), 199–230. [https://doi.org/10.1016/0377-0273\(80\)90105-5](https://doi.org/10.1016/0377-0273(80)90105-5).
- Miyabuchi, Y., 2009. A 90,000-year tephrostratigraphic framework of Aso Volcano, Japan. *Sediment. Geol.* 220 (3–4), 169–189. <https://doi.org/10.1016/j.sedgeo.2009.04.018>.
- Miyabuchi, Y., 2011. Post-caldera explosive activity inferred from improved 67–30 ka tephrostratigraphy at Aso Volcano, Japan. *J. Volcanol. Geoth. Res.* 205 (3–4), 94–113. <https://doi.org/10.1016/j.jvolgeores.2011.05.004>.
- Moore, G., Marone, C., Carmichael, I.S., Renne, P., 1994. Basaltic volcanism and extension near the intersection of the Sierra Madre volcanic province and the Mexican Volcanic Belt. *Geol. Soc. Am. Bull.* 106 (3), 383–394. [https://doi.org/10.1130/0016-7606\(1994\)106<0383:BVAENT>2.3.CO;2](https://doi.org/10.1130/0016-7606(1994)106<0383:BVAENT>2.3.CO;2).
- Müller, W., Shelley, M., Miller, P., Broude, S., 2009. Initial performance metrics of a new custom-designed ArF excimer LA-ICPMS system coupled to a two-volume laser-ablation cell. *J. Anal. Atom. Spectrom.* 24 (2), 209–214. <https://doi.org/10.1039/B805995K>.
- Nixon, G.T., 1982. The relationship between Quaternary volcanism in central Mexico and the seismicity and structure of subducted ocean lithosphere. *Geol. Soc. Am. Bull.* 93 (6), 514–523. [https://doi.org/10.1130/0016-7606\(1982\)93<514:TRBQVI>2.0.CO;2](https://doi.org/10.1130/0016-7606(1982)93<514:TRBQVI>2.0.CO;2).
- Paton, C., Hellstrom, J., Paul, B., Woodhead, J., Hergt, J., 2011. Iolite: freeware for the visualisation and processing of mass spectrometric data. *J. Anal. Atom. Spectrom.* 26 (12), 2508–2518. <https://doi.org/10.1039/C1JA10172B>.
- Phillips, E.H., Goff, F., Kyle, P.R., McIntosh, W.C., Dunbar, N.W., Gardner, J.N., 2007. The 40Ar/39Ar age constraints on the duration of resurgence at the Valles caldera, New Mexico. *J. Geophys. Res.: Solid Earth* 112 (B8). <https://doi.org/10.1029/2006JB004511>.
- Rivera Olguín, E., 2016. Historia eruptiva del Volcán Planillas: vulcanismo post caldera en la caldera de La Primavera, Jal. <http://nинive.uaslp.mx/xmlui/handle/1/4095>.
- Rosas-Elguera, J., Ferrari, L., Martínez, M.L., Urrutia-Fucugauchi, J., 1997. Stratigraphy and tectonics of the Guadalajara region and triple-junction area, western Mexico. *Int. Geol. Rev.* 39 (2), 125–140. <https://doi.org/10.1080/00206819709465263>.
- Rossotti, A., Ferrari, L., Martínez, M.L., Elguera, J.R., 2002. Geology of the boundary between the Sierra Madre Occidental and the Trans-Mexican volcanic Belt in the Guadalajara region, western Mexico. *Rev. Mex. Ciencias Geol.* 19 (1), 1–15.
- Santoyo-Gutiérrez, S., García, A., Morales, M., Perezyera, J., Rosas, A., 1991. Applied technology in the solution of geothermal drilling problems of deep wells in La Primavera caldera (Mexico). *J. Volcanol. Geoth. Res.* 47 (1–2), 195–208. [https://doi.org/10.1016/0377-0273\(91\)90109-D](https://doi.org/10.1016/0377-0273(91)90109-D).
- Sohn, Y.K., Chough, S.K., 1989. Depositional processes of the Suwolbong tuff ring, Cheju Island (Korea). *Sedimentology* 36 (5), 837–855. <https://doi.org/10.1111/j.1365-3091.1989.tb01749.x>.
- Solari, L.A., Gómez-Tuena, A., Bernal, J.P., Pérez-Arvizu, O., Tanner, M., 2010. U-Pb zircon geochronology with an integrated LA-ICP-MS microanalytical workstation: achievements in precision and accuracy. *Geostand. Geoanal. Res.* 34 (1), 5–18. <https://doi.org/10.1111/j.1751-908X.2009.00027.x>.
- Smith, R.L., Bailey, R.A., 1968. Stratigraphy, structure, and volcanic evolution of the Jemez Mountains, New Mexico. *Spec. Pap. Geol. Soc. Am.* 447–448. <https://doi.org/10.1130/MEM116-p613>.
- Tinoco Murillo, Z.S., 2017. Génesis y mecanismos de emplazamiento de la pómex gigante de la Caldera de La Primavera, Jalisco. <https://coleccióndigital.cemiego.org/xmlui/handle/123456789/537>.
- Vazquez, J.A., Velasco, N.O., Schmitt, A.K., Bleick, H.A., Stelten, M.E., 2014. 238U–230Th dating of chevkinite in high-silica rhyolites from La Primavera and Yellowstone calderas. *Chem. Geol.* 390, 109–118. <https://doi.org/10.1016/j.chemgeo.2014.10.020>.
- Vermeesch, P., 2018. IsoplotR: a free and open toolbox for geochronology. *Geosci. Front.* 9 (5), 1479–1493. <https://doi.org/10.1016/j.gsf.2018.04.001>.
- Walker, G.P.L., Wright, J.V., Clough, B.J., Booth, B., 1981. Pyroclastic geology of the rhyolitic volcano of La Primavera, Mexico. *Geol. Rundsch.* 70 (3), 1100–1118. <https://doi.org/10.1007/BF01820184>.
- Wolff, J.A., Gardner, J.N., 1995. Is the Valles caldera entering a new cycle of activity? *Geology* 23 (5), 411–414. [https://doi.org/10.1130/0091-7613\(1995\)023<411:ITVCEA>2.3.CO;2](https://doi.org/10.1130/0091-7613(1995)023<411:ITVCEA>2.3.CO;2).